$$\begin{cases} if \frac{1}{3}\sum_{n=0}^{2} pUPDs_n > \frac{1}{3}\sum_{n=0}^{2} mUPD_n \\ then \frac{1}{3}\sum_{n=0}^{2} pUPDs_n > \frac{1}{3}\sum_{n=0}^{2} Leukocytes_n > \frac{1}{3}\sum_{n=0}^{2} mUPD_n \\ if \frac{1}{3}\sum_{n=0}^{2} mUPD_n > \frac{1}{3}\sum_{n=0}^{2} pUPDs_n \\ then \frac{1}{3}\sum_{n=0}^{2} mUPD_n > \frac{1}{3}\sum_{n=0}^{2} Leukocytes_n > \frac{1}{3}\sum_{n=0}^{2} pUPDs_n. \end{cases}$$

The final condition was that the average of three consecutive probes for normal leukocytes is within the 0.25–0.75 intermediate methylation range:

$$0.25 > \frac{1}{3}\sum_{n=0}^{2} Leukocytes_n > 0.75.$$

Genotyping and imprinting analysis

Genotypes of potential SNPs identified in the UCSC Genome Browser (hg19) were obtained by PCR and direct sequencing. Sequence traces were interrogated using Sequencher v4.6 (Gene Codes Corporation) to distinguish heterozygous and homozygous samples. Heterozygous sample sets were analyzed for either allelic expression using RT-PCR or bisulfite PCR, incorporating the polymorphism within the final PCR amplicon so that parental alleles could be distinguished (for primer sequence, see Supplemental Table S3).

Bisulfite PCR

Approximately 1 μg DNA was subjected to sodium bisulfite treatment and purified using the EZ DNA Methylation-Gold kit (Zymo), and was used for all bisulfite PCR analysis. Approximately 2 μL of bisulfite-converted DNA was used in each amplification reaction using Immolase Taq polymerase (Bioline) at 35–45 cycles, and the resulting PCR product cloned into pGEM-T easy vector (Promega) for subsequent subcloning and sequencing (for primer sequence, see Supplemental Table S3). For the confirmation of an imprinted DMR, we analyzed a minimum of three heterozygous samples and, where possible, two different tissues.

Chromatin immunoprecipitation (ChIP)

We analyzed publicly available H3K4me3 ChIP-seq and meDIP-seq data sets, including those derived from lymphocytes (GSM772948, GSM772836, GSM772916, GSM543025, GSM613913), brain (GSM806943, GSM806935, GSM806948, GSM669614, GSM669615), and the H1 hES cell line (GSM409308, GSM469971, GSM605315, GSM428289, GSM456941, GSM543016). For H3K9me3 in hES cells, we used GSM450266. In addition, we used the sperm ChIP-seq data set for H3K4me3 as a direct measure of nucleosome occupancy (GSM392696, GSM392697, GSM392698, GSM392714, GSM392715, GSM392716) (Hammoud et al. 2009).

The confirmation of allelic H3K4me3 in leukocytes or lymphoblastoid cell lines was performed as previously described (Iglesias-Platas et al. 2013). Briefly, 100 μg of chromatin was used for an immunoprecipitation reaction with Protein A agarose/salmon sperm DNA (16-157, Millipore) and a H3K4me3 (07-473, Millipore). Each ChIP was performed in triplicate alongside a mock immunoprecipitation with an unrelated IgG antiserum, and a 1% fraction of the input chromatin was extracted in parallel. Levels of immunoprecipitated chromatin at each specific region were determined by qPCR using SYBR Green (Applied Biosystems) carried out on the Applied Biosystems 7900 Fast real-time PCR system (for primer sequence, see Supplemental Table S3). Each PCR was run in triplicate and protein binding was quantified as a percentage of total input material.

Data access

The data from this study have been submitted to the NCBI Gene Expression Omnibus (GEO; http://www.ncbi.nlm.nih.gov/geo/) under accession number GSE52578.

List of affiliations

[1]Imprinting and Cancer Group, Cancer Epigenetic and Biology Program, Institut d'Investigació Biomedica de Bellvitge, Hospital Duran i Reynals, 08908 Barcelona, Spain; [2]Department of Maternal-Fetal Biology, National Research Institute for Child Health and Development, Tokyo 157-8535, Japan; [3]Servicio de Neonatología, Hospital Sant Joan de Déu, Fundació Sant Joan de Déu, 08950 Barcelona, Spain; [4]Department of Systems Biomedicine, National Research Institute for Child Health and Development, Tokyo 157-8535, Japan; [5]Fundación IVI-Instituto Universitario IVI-Universidad de Valencia, INCLIVA, 46980 Paterna, Valencia, Spain; [6]Centre for Stem Cell Biology, Department of Biomedical Science, University of Sheffield, Sheffield S10 2TN, United Kingdom; [7]Reeve-Irvine Research Centre, Sue and Bill Gross Stem Cell Research Center, Department of Anatomy and Neurobiology, School of Medicine, University of California at Irvine, Irvine, California 92697, USA; [8]Cancer Epigenetics Group, Cancer Epigenetic and Biology Program, Institut d'Investigació Biomedica de Bellvitge, Hospital Duran i Reynals, 08908 Barcelona, Spain; [9]Department of Obstetrics and Gynecology, Graduate School of Medical Science, Kyushu University, Fukuoka 812-8582, Japan; [10]Instituto de Genética Médica y Molecular, CIBERER, IDIPAZ-Hospital Universitario La Paz, Universidad Autónoma de Madrid, 28046 Madrid, Spain; [11]Division of Molecular Genetics and Epigenetics, Department of Biomolecular Sciences, Faculty of Medicine, Saga University, Saga 849-8501, Japan; [12]Department of Physiological Sciences II, School of Medicine, University of Barcelona, 08036 Barcelona, Catalonia, Spain; [13]Institucio Catalana de Recerca i Estudis Avançats (ICREA), 08010 Barcelona, Catalonia, Spain; [14]Department of Pediatrics, Hamamatsu University School of Medicine, Hamamatsu 431-3192, Japan.

Acknowledgments

We thank S. Morán at PEBC-IDIBELL for performing the methylation array hybridization and S. Sayols and H. Heyn for bioinformatics assistance. We also thank P. Arnaud and J. Frost for stimulating discussions and helpful comments. This work was partially funded by grants from the Fundació La Marató de TV3 (grant no. 101130 to D.M. and P.L.); Spanish Ministerio de Educacion y Ciencia (BFU2011-27658 to D.M.); JST/CREST and the Health and Labour Sciences Research Grant (Nanbyo-Ippan-003 to K.H.); the Ministry of Education, Culture, Sports, Science, and Technology of Japan (#22249010) and the National Center for Child Health and Development (#24-3) to K.N. D.M. is a Ramon y Cajal research fellow. Finally, we would like to thank all the patients and their families for participating in this project.

References

Amor DJ, Halliday J. 2008. A review of known imprinting syndromes and their association with assisted reproduction technologies. *Hum Reprod* **23:** 2826–2834.

Baglivo I, Esposito S, De Cesare L, Sparago A, Anvar Z, Riso V, Cammisa M, Fattorusso R, Grimaldi G, Riccio A, et al. 2013. Genetic and epigenetic mutations affect the DNA binding capability of human ZFP57 in transient neonatal diabetes type 1. *FEBS Lett* **587:** 1474–1481.
Barbaux S, Gascoin-Lachambre G, Buffat C, Monnier P, Mondon F, Tonanny MB, Pinard A, Auer J, Bessières B, Barlier A, et al. 2012. A genome-wide approach reveals novel imprinted genes expressed in the human placenta. *Epigenetics* **7:** 1079–1090.
Bourc'his D, Xu GL, Lin CS, Bollman B, Bestor TH. 2001. Dnmt3L and the establishment of maternal genomic imprints. *Science* **294:** 2536–2539.
Buiting K. 2010. Prader-Willi syndrome and Angelman syndrome. *Am J Med Genet C Semin Med Genet* **154C:** 365–376.
Choufani S, Shuman C, Weksberg R. 2010. Beckwith-Wiedemann syndrome. *Am J Med Genet C Semin Med Genet* **154C:** 343–354.
Ciccone DN, Su H, Hevi S, Gay F, Lei H, Bajko J, Xu G, Li E, Chen T. 2009. KDM1B is a histone H3K4 demethylase required to establish maternal genomic imprints. *Nature* **461:** 415–418.
Constância M, Kelsey G, Reik W. 2004. Resourceful imprinting. *Nature* **432:** 53–57.
Coombes C, Arnaud P, Gordon E, Dean W, Coar EA, Williamson CM, Feil R, Peters J, Kelsey G. 2003. Epigenetic properties and identification of an imprint mark in the Nesp-Gnasxl domain of the mouse *Gnas* imprinted locus. *Mol Cell Biol* **23:** 5475–5488.
Cooper WN, Constância M. 2010. How genome-wide approaches can be used to unravel the remaining secrets of the imprintome. *Brief Funct Genomics* **9:** 315–328.
Das R, Lee YK, Strogantsev R, Jin S, Lim YC, Ng PY, Lin XM, Chng K, Yeo GSh, Ferguson-Smith AC, et al. 2013. DNMT1 and AIM1 imprinting in human placenta revealed through a genome-wide screen for allele-specific DNA methylation. *BMC Genomics* **14:** 685.
Dhayalan A, Rajavelu A, Rathert P, Tamas R, Jurkowska RZ, Ragozin S, Jeltsch A. 2010. The Dnmt3a PWWP domain reads histone 3 lysine 36 trimethylation and guides DNA methylation. *J Biol Chem* **285:** 26114–26120.
Eggermann T. 2010. Russell-Silver syndrome. *Am J Med Genet C Semin Med Genet* **154C:** 355–364.
Ehrlich M, Gama-Sosa MA, Huang LH, Midgett RM, Kuo KC, McCune RA, Gehrke C. 1982. Amount and distribution of 5-methylcytosine in human DNA from different types of tissues of cells. *Nucleic Acids Res* **10:** 2709–2721.
El-Maarri O, Buiting K, Peery EG, Kroisel PM, Balaban B, Wagner K, Urman B, Heyd J, Lich C, Brannan CI, et al. 2001. Maternal methylation imprints on human chromosome 15 are established during or after fertilization. *Nat Genet* **27:** 41–44.
Fuke C, Shimabukuro M, Petronis A, Sugimoto J, Oda T, Miura K, Miyazaki T, Ogura C, Okazaki Y, Jinno Y. 2004. Age related changes in 5-methylcytosine content in human peripheral leukocytes and placentas: An HPLC-based study. *Ann Hum Genet* **68:** 196–204.
Geuns E, De Temmerman N, Hilven P, Van Steirteghem A, Liebaers I, De Rycke M. 2007. Methylation analysis of the intergenic differentially methylated region of DLK1-GTL2 in human. *Eur J Hum Genet* **15:** 352–361.
Gregg C, Zhang J, Weissbourd B, Luo S, Schroth GP, Haig D, Dulac C. 2010. High-resolution analysis of parent-of-origin allelic expression in the mouse brain. *Science* **329:** 643–648.
Hammoud SS, Nix DA, Zhang H, Purwar J, Carrell DT, Cairns BR. 2009. Distinctive chromatin in human sperm packages genes for embryo development. *Nature* **460:** 473–478.
Harness JV, Turovets NA, Seiler MJ, Nistor G, Altun G, Agapova LS, Ferguson D, Laurent LC, Loring JF, Keirstead HS. 2011. Equivalence of conventionally-derived and parthenote-derived human embryonic stem cells. *PLoS ONE* **6:** e14499.
Hata K, Okano M, Lei H, Li E. 2002. Dnmt3L cooperates with the Dnmt3 family of de novo DNA methyltransferases to establish maternal imprints in mice. *Development* **129:** 1983–1993.
Hayashizaki Y, Shibata H, Hirotsune S, Sugino H, Okazaki Y, Sasaki N, Hirose K, Imoto H, Okuizumi H, Muramatsu M, et al. 1994. Identification of an imprinted U2af binding protein related sequence on mouse chromosome 11 using the RLGS method. *Nat Genet* **6:** 33–40.
Heyn H, Li N, Ferreira HJ, Moran S, Pisano DG, Gomez A, Diez J, Sanchez-Mut JV, Setien F, Carmona FJ, et al. 2012. Distinct DNA methylomes of newborns and centenarians. *Proc Natl Acad Sci* **109:** 10522–10527.
Hiura H, Sugawara A, Ogawa H, John RM, Miyauchi N, Miyanari Y, Horiike T, Li Y, Yaegashi N, Sasaki H, et al. 2010. A tripartite paternally methylated region within the *Gpr1-Zdbf2* imprinted domain on mouse chromosome 1 identified by meDIP-on-chip. *Nucleic Acids Res* **38:** 4929–4945.
Kanber D, Berulava T, Ammerpohl O, Mitter D, Richter J, Siebert R, Horsthemke B, Lohman D, Buiting K. 2009. The human retinoblastoma gene is imprinted. *PLoS Genet* **12:** e1000790.
Iglesias-Platas I, Court F, Camprubi C, Sparago A, Guillaumet-Adkins A, Martin-Trujillo A, Riccio A, Moore GE, Monk D. 2013. Imprinting at the *PLAGL1* domain is contained within a 70-kb CTCF/cohesin-mediated non-allelic chromatin loop. *Nucleic Acids Res* **41:** 2171–2179.
Kagami M, Sekita Y, Nishimura G, Irie M, Kato F, Okada M, Yamamori S, Kishimoto H, Nakayama M, Tanaka Y, et al. 2008. Deletions and epimutations affecting the human 14q32.2 imprinted region in individuals with paternal and maternal upd(14)-like phenotypes. *Nat Genet* **40:** 237–242.
Kagami M, O'Sullivan MJ, Green AJ, Watabe Y, Arisaka O, Masawa N, Matsuoka K, Fukami M, Matsubara K, Kato F, et al. 2010. The IG-DMR and the *MEG3*-DMR at human chromosome 14q32.2: Hierarchical interaction and distinct functional properties as imprinting control centers. *PLoS Genet* **6:** e1000992.
Kelsey G. 2010. Imprinting on chromosome 20: Tissue-specific imprinting and imprinting mutations in the GNAS locus. *Am J Med Genet C Semin Med Genet* **154C:** 377–386.
Kelsey G, Bodle D, Miller HJ, Beechey CV, Coombes C, Peters J, Williamson CM. 1999. Identification of imprinted loci by methylation-sensitive representational difference analysis: Application to mouse distal chromosome 2. *Genomics* **62:** 129–138.
Kobayashi H, Sakurai T, Imai M, Takahashi N, Fukuda A, Yayoi O, Sato S, Nakabayashi K, Hata K, Sotomaru Y, et al. 2012. Contribution of intragenic DNA methylation in mouse gametic DNA methylomes to establish oocyte-specific heritable marks. *PLoS Genet* **8:** e1002440.
Kobayashi H, Yanagisawa E, Sakashita A, Sugawara N, Kumakura S, Ogawa H, Akutsu H, Hata K, Nakabayashi K, Kono T. 2013. Epigenetic and transcriptional features of the novel human imprinted lncRNA *GPR1AS* suggest it is a functional ortholog to mouse *Zdbf2linc*. *Epigenetics* **8:** 635–645.
Kong A, Steinthorsdottir V, Masson G, Thorleifsson G, Sulem P, Besenbacher S, Jonasdottir A, Sigurdsson A, Kristinsson KT, Jonasdottir A, et al. 2009. Parental origin of sequence variants associated with complex diseases. *Nature* **462:** 868–874.
Lapunzina P, Monk D. 2011. The consequences of uniparental disomy and copy number neutral loss-of-heterozygosity during human development and cancer. *Biol Cell* **103:** 303–317.
Li X, Ito M, Zhou F, Youngson N, Zuo X, Leder P, Ferguson-Smith AC. 2008. A maternal-zygotic effect gene, *Zfp57*, maintains both maternal and paternal imprints. *Dev Cell* **15:** 547–557.
Lister R, Pelizzola M, Dowen RH, Hawkins RD, Hon G, Tonti-Filippini J, Nery JR, Lee L, Ye Z, Ngo QM, et al. 2009. Human DNA methylomes at base resolution show widespread epigenomic differences. *Nature* **462:** 315–322.
Lopes S, Lewis A, Hajkova P, Dean W, Oswald J, Forné T, Murrell A, Constância M, Bartolomei M, Walter J, et al. 2003. Epigenetic modifications in an imprinting cluster are controlled by a hierarchy of DMRs suggesting long-range chromatin interactions. *Hum Mol Genet* **12:** 295–305.
Mackay DJ, Temple IK. 2010. Transient neonatal diabetes mellitus type 1. *Am J Med Genet C Semin Med Genet* **154C:** 335–342.
Mai Q, Yu Y, Li T, Wang L, Chen MJ, Huang SZ, Zhou C, Zhou Q. 2007. Derivation of human embryonic stem cell lines from parthenogenetic blastocysts. *Cell Res* **17:** 1008–1012.
Molaro A, Hodges E, Fang F, Song Q, McCombie WR, Hannon GJ, Smith AD. 2011. Sperm methylation profiles reveal features of epigenetic inheritance and evolution in primates. *Cell* **146:** 1029–1041.
Monk D. 2010. Deciphering the cancer imprintome. *Brief Funct Genomics* **9:** 329–339.
Monk D, Arnaud P, Apostolidou S, Hills FA, Kelsey G, Stanier P, Feil R, Moore GE. 2006. Limited evolutionary conservation of imprinting in the human placenta. *Proc Natl Acad Sci* **103:** 6623–6628.
Nakabayashi K, Trujillo AM, Tayama C, Camprubi C, Yoshida W, Lapunzina P, Sanchez A, Soejima H, Aburatani H, Nagae G, et al. 2011. Methylation screening of reciprocal genome-wide UPDs identifies novel human-specific imprinted genes. *Hum Mol Genet* **20:** 3188–3197.
Nakamura T, Arai Y, Umehara H, Masuhara M, Kimura T, Taniguchi H, Sekimoto T, Ikawa M, Yoneda Y, Okabe M. 2007. PGC7/Stella protects against DNA demethylation in early embryogenesis. *Nat Cell Biol* **9:** 64–71.
Noguer-Dance M, Abu-Amero S, Al-Khtib M, Lefèvre A, Coullin P, Moore GE, Cavaillé J. 2010. The primate-specific microRNA gene cluster (C19MC) is imprinted in the placenta. *Hum Mol Genet* **19:** 3566–3582.
Okae H, Hiura H, Nishida Y, Funayama R, Tanaka S, Chiba H, Yaegashi N, Nakayama K, Sasaki H, Arima T. 2011. Re-investigation and RNA sequencing-based identification of genes with placenta-specific imprinted expression. *Hum Mol Genet* **21:** 548–558.
Park KY, Sellars EA, Grinberg A, Huang SP, Pfeifer K. 2004. The H19 differentially methylated region marks the parental origin of a heterologous locus without gametic DNA methylation. *Mol Cell Biol* **24:** 3588–3595.
Proudhon C, Duffié R, Ajjan S, Cowley M, Iranzo J, Carbajosa G, Saadeh H, Holland ML, Oakey RJ, Rakyan VK, et al. 2012. Protection against de

novo methylation is instrumental in maintaining parent-of-origin methylation inherited from the gametes. *Mol Cell* **47:** 909–920.
Quenneville S, Verde G, Corsinotti A, Kapopoulou A, Jakobsson J, Offner S, Baglivo I, Pedone PV, Grimaldi G, Riccio A, et al. 2011. In embryonic stem cells, ZFP57/KAP1 recognize a methylated hexanucleotide to affect chromatin and DNA methylation of imprinting control regions. *Mol Cell* **44:** 361–372.
Ramowitz LK, Bartolomei MS. 2011. Genomic imprinting: Recognition and marking of imprinted loci. *Curr Opin Genet Dev* **22:** 72–78.
Romanelli V, Nevado J, Fraga M, Trujillo AM, Mori MÁ, Fernández L, Pérez de Nanclares G, Martínez-Glez V, Pita G, Meneses H, et al. 2011. Constitutional mosaic genome-wide uniparental disomy due to diploidisation: An unusual cancer-predisposing mechanism. *J Med Genet* **48:** 212–216.
Schroeder DI, Blair JD, Lott P, Yu HO, Hong D, Crary F, Ashwood P, Walker C, Korf I, Robinson WP, et al. 2013. The human placenta methylome. *Proc Natl Acad Sci* **110:** 6037–6042.
Sharp A, Migliavacca E, Dupre Y, Stathaki E, Reza Sailani M, Baumer A, Schinzel A, Mackay DJ, Robinson DO, Cobellis G, et al. 2010. Methylation profiling in individuals with uniparental disomy identify novel differentially methylated regions on chromosome 15. *Genome Res* **20:** 1271–1278.
Smallwood SA, Tomizawa S, Krueger F, Ruf N, Carli N, Segonds-Pichon A, Sato S, Hata K, Andrews SR, Kelsey G. 2011. Dynamic CpG island methylation landscape in oocytes and pre-implantation embryos. *Nat Genet* **43:** 811–814.
Smith ZD, Chan MM, Mikkelsen TS, Gu H, Gnirke A, Regev A, Meissner A. 2012. A unique regulatory phase of DNA methylation in the early mammalian embryo. *Nature* **484:** 339–344.
Thomson JP, Skene PJ, Selfridge J, Clouaire T, Guy J, Webb S, Kerr AR, Deaton A, Andrews R, James KD, et al. 2010. CpG islands influence chromatin structure via the CpG-binding protein Cfp1. *Nature* **464:** 1082–1086.
Tomizawa S, Kobayashi H, Watanabe T, Andrews S, Hata K, Kelsey G, Sasaki H. 2011. Dynamic stage-specific changes in imprinted differentially methylated regions during early mammalian development and prevalence of non-CpG methylation in oocytes. *Development* **138:** 811–820.
Umlauf D, Goto Y, Cao R, Cerqueira F, Wagschal A, Zhang Y, Feil R. 2004. Imprinting along the *Kcnq1* domain on mouse chromosome 7 involves repressive histone methylation and recruitment of Polycomb group complexes. *Nat Genet* **36:** 1296–1300.
Wood AJ, Schulz R, Woodfine K, Koltowska K, Beechey CV, Peters J, Bourc'his D, Oakey RJ. 2008. Regulation of alternative polyadenylation by genomic imprinting. *Genes Dev* **22:** 1141–1146.
Xie W, Barr CL, Kim A, Yue F, Lee AY, Eubanks J, Dempster EL, Ren B. 2012. Base-resolution analyses of sequence and parent-of-origin dependent DNA methylation in the mouse genome. *Cell* **148:** 816–831.
Yamazawa K, Nakabayashi K, Kagami M, Sato T, Saitoh S, Horikawa R, Hizuka N, Ogata T. 2010. Parthenogenetic chimaerism/mosaicism with a Silver-Russell syndrome-like phenotype. *J Med Genet* **47:** 782–785.
Yuen RKC, Jiang R, Penaherrera M, McFadeen DE, Robinson WP. 2011. Genome-wide mapping of imprinted differentially methylated regions by DNA methylation profiling of human placentas from triploidies. *Epigenetics & Chromatin* **4:** 10.
Zeng J, Konopka G, Hunt BG, Preuss TM, Geschwind D, Yi SV. 2012. Divergent whole-genome methylation maps of human and chimpanzee brains reveal epigenetic basis of human regulatory evolution. *Am J Hum Genet* **91:** 455–465.
Zhang Y, Jurkowska R, Soeroes S, Rajavelu A, Dhayalan A, Bock I, Rathert P, Brandt O, Reinhardt R, Fischle W, et al. 2010. Chromatin methylation activity of Dnmt3a and Dnmt3a/3L is guided by interaction of the ADD domain with the histone H3 tail. *Nucleic Acids Res* **38:** 4246–4253.

Received August 9, 2013; accepted in revised form December 26, 2013.

Cell

Premature Termination of Reprogramming In Vivo Leads to Cancer Development through Altered Epigenetic Regulation

Kotaro Ohnishi,[1,2,8] Katsunori Semi,[1,3,8] Takuya Yamamoto,[1,3] Masahito Shimizu,[2] Akito Tanaka,[1] Kanae Mitsunaga,[1] Keisuke Okita,[1] Kenji Osafune,[1] Yuko Arioka,[1] Toshiyuki Maeda,[4] Hidenobu Soejima,[4] Hisataka Moriwaki,[2] Shinya Yamanaka,[1,3,5] Knut Woltjen,[1,6] and Yasuhiro Yamada[1,3,7,*]

[1]Center for iPS Cell Research and Application (CiRA), Kyoto University, Kyoto 606-8507, Japan
[2]Department of Medicine, Gifu University Graduate School of Medicine, Gifu 501-1194, Japan
[3]Institute for Integrated Cell-Material Sciences (WPI-iCeMS), Kyoto University, Kyoto 606-8507, Japan
[4]Division of Molecular Genetics and Epigenetics, Department of Biomolecular Sciences, Faculty of Medicine, Saga University, Saga 849-8501, Japan
[5]Gladstone Institute of Cardiovascular Disease, San Francisco, CA 94158, USA
[6]Hakubi Center for Advanced Research, Kyoto University, Kyoto 606-8507, Japan
[7]PRESTO, Japan Science and Technology Agency, 4-1-8 Honcho Kawaguchi, Saitama, 332-0012, Japan
[8]These authors contributed equally to this work
*Correspondence: y-yamada@cira.kyoto-u.ac.jp
http://dx.doi.org/10.1016/j.cell.2014.01.005

SUMMARY

Cancer is believed to arise primarily through accumulation of genetic mutations. Although induced pluripotent stem cell (iPSC) generation does not require changes in genomic sequence, iPSCs acquire unlimited growth potential, a characteristic shared with cancer cells. Here, we describe a murine system in which reprogramming factor expression in vivo can be controlled temporally with doxycycline (Dox). Notably, transient expression of reprogramming factors in vivo results in tumor development in various tissues consisting of undifferentiated dysplastic cells exhibiting global changes in DNA methylation patterns. The Dox-withdrawn tumors arising in the kidney share a number of characteristics with Wilms tumor, a common pediatric kidney cancer. We also demonstrate that iPSCs derived from Dox-withdrawn kidney tumor cells give rise to nonneoplastic kidney cells in mice, proving that they have not undergone irreversible genetic transformation. These findings suggest that epigenetic regulation associated with iPSC derivation may drive development of particular types of cancer.

INTRODUCTION

Induced pluripotent stem cells (iPSCs) can be established from differentiated somatic cells by the forced induction of four transcription factors: *Oct3/4*, *Klf4*, *Sox2*, and *c-Myc* (Takahashi et al., 2007; Takahashi and Yamanaka, 2006; Maherali et al., 2007; Okita et al., 2007; Wernig et al., 2007; Woltjen et al., 2009). To achieve somatic cell reprogramming, multiple cellular processes act synergistically in a sequential manner (Brambrink et al., 2008; Polo et al., 2012; Samavarchi-Tehrani et al., 2010). Despite extensive studies, the precise mechanism of somatic cell reprogramming still remains unclear (Rais et al., 2013). It is known that non-iPSC-like colonies often appear at the intermediate stage of cellular reprogramming in vitro. In addition, there are several reports describing partial iPSCs that deviate successful reprogramming (Fussner et al., 2011; Mikkelsen et al., 2008; Sridharan et al., 2009). However, the characteristics of such failed reprogramming states are largely unknown, and no study has elucidated the failed reprogramming state from cell types other than fibroblasts.

The process of iPSC derivation shares many characteristics with cancer development. During reprogramming, somatic differentiated cells acquire the properties of self-renewal along with unlimited proliferation and exhibit global alterations of the transcriptional program, which are also critical events during carcinogenesis (Ben-Porath et al., 2008). The metabolic switch to glycolysis that occurs during somatic cell reprogramming is similarly observed in cancer development (Folmes et al., 2011). Such similarities suggest that reprogramming processes and cancer development may be partly promoted by overlapping mechanisms (Hong et al., 2009). Practically, the forced induction of the critical reprogramming factor *Oct3/4* in adult somatic cells results in dysplastic growth in epithelial tissues through the inhibition of cellular differentiation in a manner similar to that in embryonic cells (Hochedlinger et al., 2005). These studies provided a possible link between transcription-factor-mediated reprogramming and cancer development.

To elucidate the involvement of failed reprogramming in cancer development, in the present study, we generated an in vivo reprogramming mouse system using reprogramming factor-inducible alleles and examined the effects of reprogramming factor expression in somatic cells in vivo. We show that failed reprogramming-associated cells behave similarly to cancer cells

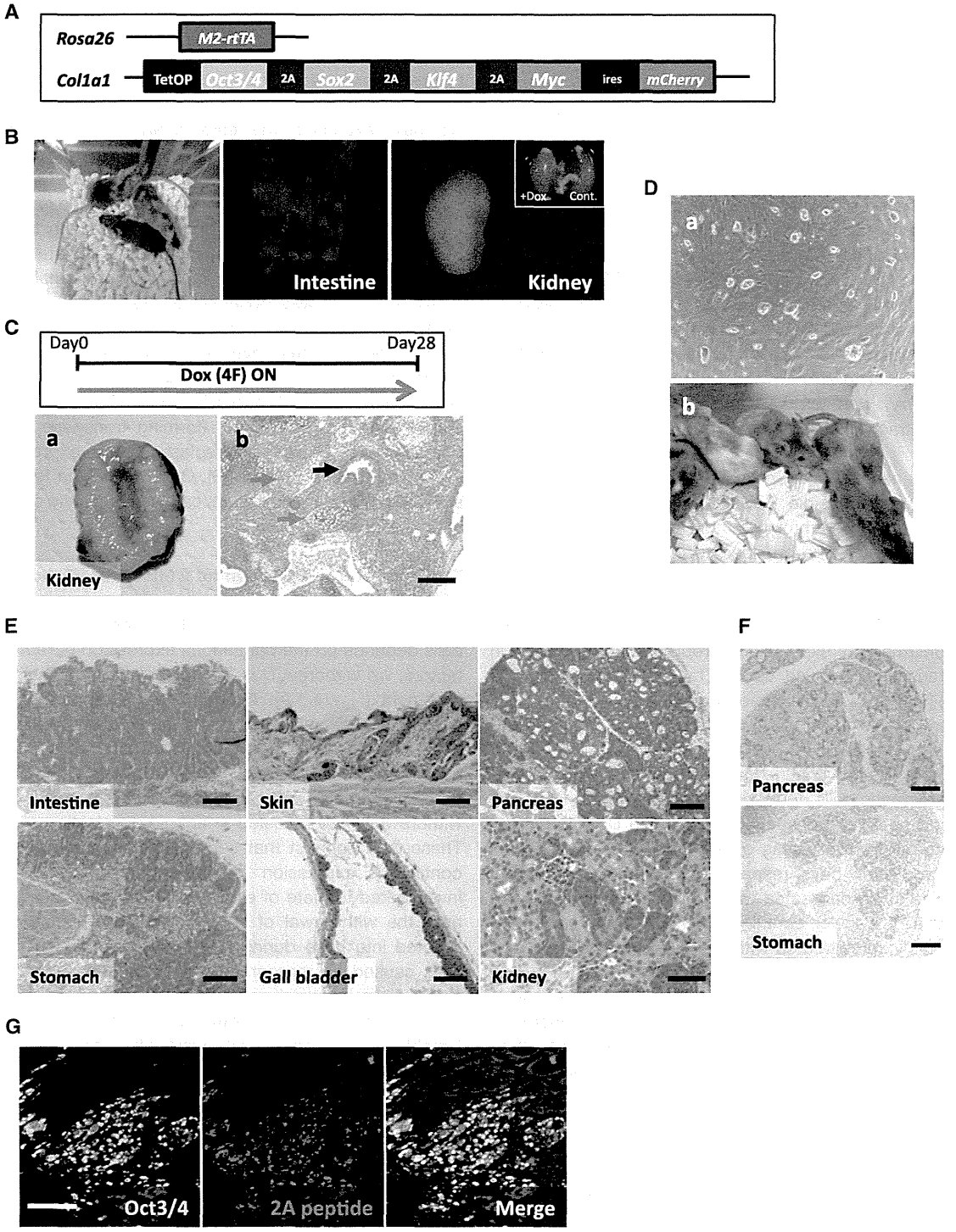

Figure 1. Reprogramming of Somatic Cells In Vivo

(A) Generation of four-factor-inducible ESCs. TetOP, tetracycline-dependent promoter.

(B) Generation of chimeric mice using OSKM-inducible ESCs. mCherry signals could be detected in various organs after Dox treatment for 3 days.

(C) Treatment of chimeric mice with Dox for 28 days resulted in the development of multiple tumors containing pluripotent stem cells. (a) A representative macroscopic image of the cut surface of the kidney tumor. (b) A histological section of the kidney tumor showing the differentiation of tumor cells into three germ layers, indicating teratoma formation. The blue, red, and black arrows represent neuronal, cartilage, and glandular epithelial components, respectively. Scale bar, 200 μm.

(legend continued on next page)

and cause neoplasia resembling Wilms tumor, a childhood blastoma in the kidney. Moreover, we demonstrate that altered epigenetic regulations cause the abnormal growth of such failed reprogramming-associated cancer cells.

RESULTS

In Vivo Reprogrammable Mouse

To establish the reprogrammable mouse system, we generated embryonic stem cells (ESCs) in which reprogramming factors can be induced under the control of doxycycline (Dox) (Figure 1A) (Carey et al., 2010; Stadtfeld et al., 2010b). We used KH2 ESCs with the optimized reverse tetracycline-dependent transactivator at the *ROSA 26* locus (Beard et al., 2006). A polycistronic cassette encoding four reprogramming factors (*Oct3/4*, *Sox2*, *Klf4*, and c-*Myc*) (Carey et al., 2010), followed by *ires-mCherry*, was targeted into the *Col1a1* gene locus under the tetracycline-dependent promoter of KH2 ESCs (Figure 1A).

Next, we generated chimeric mice via blastocyst injection of four-factor (4F)-inducible ESCs. To confirm inducible expression of the reprogramming factors and mCherry in vivo, Dox-containing water was provided to chimeric mice starting at 4 weeks of age. On day 3 of Dox treatment, we could detect the mCherry signal in various organs, including stomach, intestine, liver, pancreas, kidney, gallbladder, and skin (Figure 1B). We also confirmed the expression of reprogramming factors in germline-transmitted mouse tissues by quantitative RT-PCR (qRT-PCR) (Figure S1A available online).

Mouse embryonic fibroblasts (MEFs) containing these reprogramming factor-inducible alleles could give rise to iPSCs after Dox treatment in vitro (Figure S1B). We next asked whether responding somatic cells could be reprogrammed in vivo. The chimeric and germline-transmitted mice given Dox-containing water (2 mg/ml) from 4 weeks of age became morbid within 7–10 days and a few days, respectively. A small proportion of chimeric mice could be treated with Dox for 4 weeks, presumably because of a lower contribution of ESCs in responding tissues. Notably, mice treated with Dox for 4 weeks developed multiple tumors in several organs, such as the kidney and pancreas (Figure 1Ca), whereas tumor formation was never observed in nontreated mice (n = 7, 7 months of age). Histological analysis revealed that these tumors differentiated into three different germ layers, indicating that they are teratomas (Figure 1Cb). When teratoma cells were cultured ex vivo in the absence of Dox (no additional 4F expressions), iPSC-like cells were established (Figure 1Da). Importantly, the teratoma-derived iPSC-like cells contributed to adult chimeric mice when they were injected into blastocysts (Figure 1Db). Therefore, we conclude that somatic cells can be reprogrammed in vivo to pluripotency in our reprogrammable mouse system.

Forced Expression of Reprogramming Factors In Vivo Leads to Rapid Expansion of Dysplastic Cells

We next examined the early changes after expression of reprogramming factors in somatic cells in vivo. After treatment of 4-week-old mice with Dox for 3–9 days, all mice developed dysplastic lesions in epithelial tissues of various organs (Figure 1E), although there were variations in severity of the phenotype among chimeras. Dysplastic cells proliferated actively, as revealed by Ki67 staining (Figure 1F). Abnormal proliferation of somatic cells was observed as early as 3 days after Dox treatment (Figure S1C), and by day 7, such dysplastic cell growth was detected even for pancreatic and kidney cells, which typically do not divide actively under physiological conditions (Figures 1E and 1F). Immunofluorescent analysis of Oct3/4 and the 2A peptide (forming transgene connections) demonstrated that the dysplastic cells expressed reprogramming factors (Figure 1G). Collectively, the forced expression of reprogramming factors caused dysplastic cell expansion of epithelial tissues in vivo.

The Fate of Early Dysplastic Cells after Withdrawal of Dox

To examine whether subsequent expansion of such dysplastic cells depends on the continuous expression of reprogramming factors, we withdrew Dox for 7 days after an initial 4- to 7-day treatment (Figure 2A). Although Dox treatment for 4–7 days caused active cell proliferation in a variety of tissues of all mice, we did not observe any dysplastic cells in some mice after withdrawal of Dox (Figure 2A; Table 1). Of particular note, mice treated with Dox for periods less than 5 days before withdrawal often revealed a lack of dysplastic cells (Table 1). These data suggest that early dysplastic cell growth requires continuous expression of reprogramming factors. We next investigated the fate of eliminated dysplastic proliferating cells after the withdrawal of Dox. Bromodeoxyuridine (BrdU) was injected into mice during Dox treatment to label proliferating cells caused by reprogramming factor expression during the first 7 days (Hochedlinger et al., 2005), and then mice were sacrificed after the withdrawal of Dox for 7 days, on day14. Notably, BrdU-labeled cells were often observed in normal-looking pancreatic and kidney tissues at day14 (Figure 2B). Furthermore, BrdU-labeled cells in the pancreatic islets also expressed insulin (Figure 2B). This suggests that the expanded cells caused by the transient expression of reprogramming factors were, at least in part, integrated into normal-looking tissues after Dox withdrawal.

(D) Teratomas contain pluripotent stem cells. (a) Ex vivo teratoma culture gave rise to iPSC-like colonies without Dox exposure. (b) Teratoma-derived iPSCs contributed to adult chimeric mice.

(E) Dysplastic cell expansion by the forced expression of reprogramming factors in vivo. The histology of various organs of mice treated with Dox for 3 to 9 days. Scale bars, 200 μm (intestine, skin, pancreas, stomach, and gall bladder) and 100 μm (kidney).

(F) Ki67 immunostaining revealed active proliferation of the dysplastic cells in the pancreas and stomach. Scale bars, 200 μm.

(G) Immunofluorescent staining for Oct3/4 and 2A peptide in the intestine of an OSKM chimeric mouse treated with Dox for 7 days. The 2A antibody used here recognizes both Oct3/4-P2A and Sox2-T2A. Dysplastic cells showed positive staining for both Oct3/4 and 2A. Scale bar, 50 μm.

See also Figure S1.

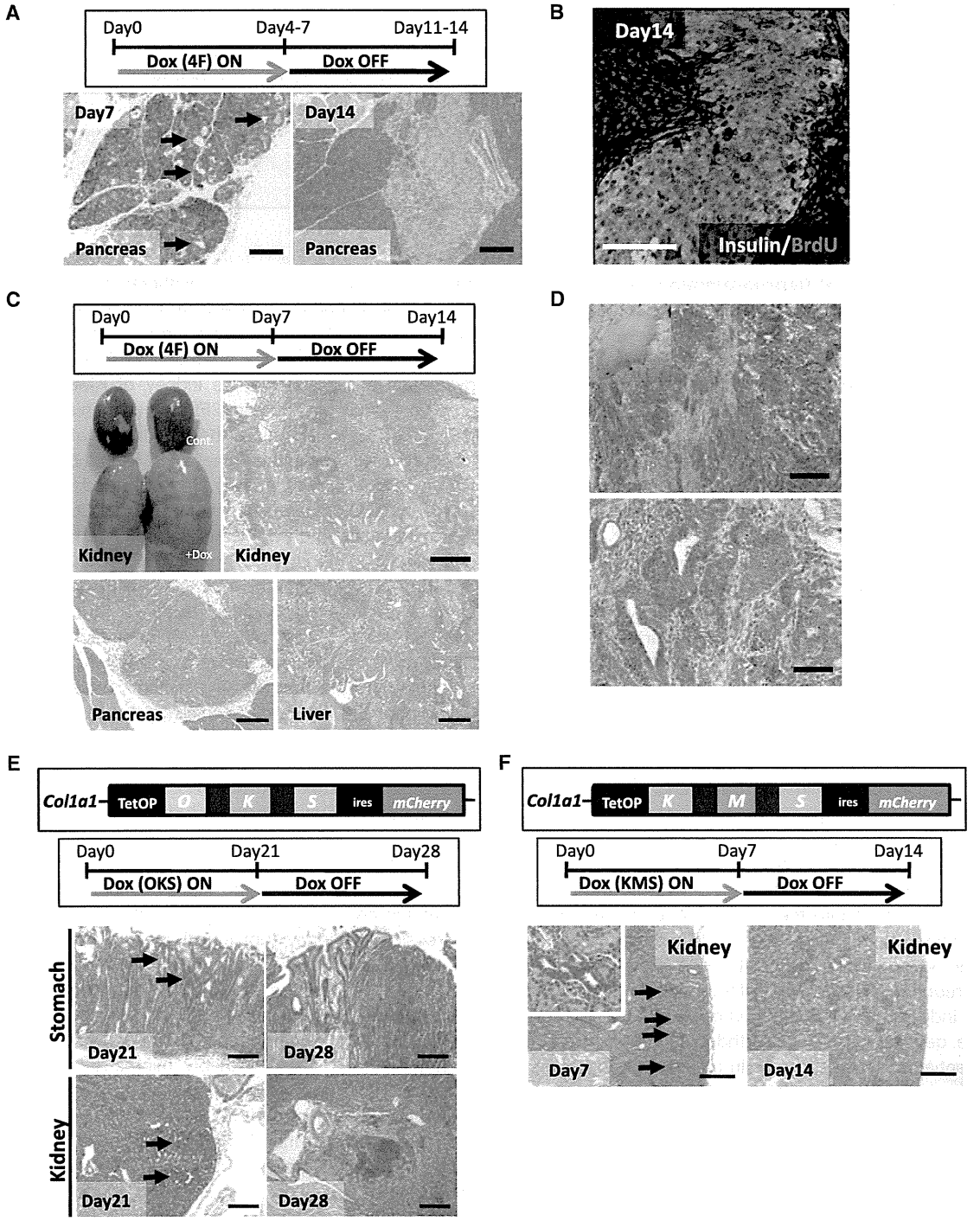

Figure 2. Transient Expression of Reprogramming Factors Causes Neoplasia

(A) A schematic drawing of the experiment and histological sections of the pancreas taken on days 7 and 14. Dysplastic cell growth was induced by treatment with Dox for 7 days (arrows on day 7). The pancreatic section taken on day 14 revealed normal histology. Scale bars, 200 μm.

(B) Double immunofluorescence for insulin and BrdU in the pancreas on day 14. For the pulse and chase experiment, BrdU was injected intraperitoneally every day during Dox administration starting on day 2 (days 2–7), followed by withdrawal of Dox for 7 days. BrdU-positive cells were frequently observed in normal-looking pancreatic islet cells, which also expressed insulin. Scale bar, 100 μm.

(C) Treatment of OSKM chimeric mice with Dox for 7 days, followed by the withdrawal of Dox for another 7 days. The macroscopic image shows the development of bilateral kidney tumors on day 14. Representative histological images are shown for Dox-withdrawn tumors in the kidney, pancreas, and liver. Scale bars, 200 μm.

(legend continued on next page)

Table1. Transient Expression of Reprogramming Factors Causes Tumor Development

		Kidney		Pancreas		Liver	
Dox Treatment	n	No Phenotype	Dysplastic Growth	No Phenotype	Dysplastic Growth	No Phenotype	Dysplastic Growth
4 days ON→OFF	4	2	2	4	0	3	1
5 days ON→OFF	2	1	1	2	0	2	0
6 days ON→OFF	5	1	4	2	3	3	2
7 days ON→OFF	33	7	26	22	11	25	8

Prolonged Expression of Reprogramming Factors Leads to Transgene-Independent Tumor Formation in Somatic Cells

In contrast to the reversion of early dysplastic proliferating cells into normal-looking cells, mice that had been given Dox for 7 days often went on to develop tumors in multiple responding organs even after Dox withdrawal (Figure 2C; Table 1). The developed tumors consisted of histologically undifferentiated dysplastic cells, which were distinct from teratoma cells (Figures 2C and S2A). The dysplastic cells invaded the surrounding tissues, which is one of the hallmarks of cancer cell growth (Figure S2A). Dox-withdrawn tumor cells were negative for 2A staining, affirming that they grew independent of transgene expression (Figure S2B). Dox-withdrawn kidney tumors were similarly observed in elderly mice given Dox starting at 14 weeks of age (13 out of 19 mice). When Dox-withdrawn kidney tumor cells were transplanted into the subcutaneous tissues of immunocompromised mice, they formed secondary tumors within 3 weeks without Dox administration (Figures 2D and S2C), reflecting the neoplastic potential of Dox-withdrawn tumor cells.

Reprogramming factors in our transgenic system include *c-Myc*, a well-known oncogene. To investigate the contribution of *c-Myc* on the development of Dox-withdrawn tumors, we generated three-factor-inducible chimeric mice, which express *Oct3/4*, *Sox2*, and *Klf4* (OKS), but not *c-Myc*, by the targeted insertion of transgenes into the identical locus as 4F (OSKM)-inducible mice (Figure 2E). Similar to 4F-induced mice, OKS induction in vivo caused dysplastic cell growth in various organs yet required longer periods of treatment (Figure 2E). After 3 weeks of induction of OKS followed by withdrawal for 7 days, these mice developed the Dox-withdrawn tumors consisting of undifferentiated dysplastic cells in multiple organs (4 out of 8 mice; Figure 2E). Therefore, transgenic *c-Myc* is dispensable for the development of Dox-withdrawn tumors.

Oct3/4 plays a critical role in cellular reprogramming, and expression of three factors (*Klf4*, *c-Myc*, and *Sox2*) in the absence of *Oct3/4* is not sufficient for iPSC generation (Takahashi and Yamanaka, 2006). To further demonstrate a link between cellular reprogramming and Dox-withdrawn tumor development, we generated chimeric mice in which *Klf4*, *c-Myc*, and *Sox2* (KMS), but not *Oct3/4*, can be induced upon Dox treatment (Figure 2F). Following Dox treatment for 7 days, we observed dysplastic cell growth in the kidney of KMS-inducible mice (three out of six mice; Figure 2F). However, in sharp contrast to OSKM/OKS-induced mice, the withdrawal of Dox eliminated the dysplastic cells in the kidney of KMS-induced mice (n = 17; Figure 2F). A previous study demonstrated that ectopic expression of *Oct3/4* alone can induce dysplastic growth whereas the transgene withdrawal leads to complete reversion of such dysplasia (Hochedlinger et al., 2005). Consistent with the previous observation, the *Oct3/4*-single induction under the same experimental condition failed to form Dox-withdrawn tumors (n = 18; Figure S2D). Taken together, we conclude that reprogramming pressure toward pluripotency driven by the combination of reprogramming factors is associated with the development of Dox-withdrawn tumors.

Loss of Cell Identity and Gain of ESC-Related Gene Expression in Dox-Withdrawn Tumors

To characterize Dox-withdrawn tumor cells, we examined gene expression in kidney tumors that arose in OSKM-inducible mice treated with the 7+/7− Dox regimen. In the KH2 system, transgene expression in the kidney is induced exclusively in the tubule cells (Beard et al., 2006). We observed decreased expression of kidney tubule cell-specific genes in Dox-withdrawn kidney tumors, indicating loss of kidney cell identity (Figure 3A). A previous study dissected the gene expression signature of ESCs into three functional modules: core pluripotency factors, Polycomb complex factors, and Myc-related factors (Kim et al., 2010). Notably, microarray analysis revealed that the ESC-Core module is similarly activated in Dox-withdrawn kidney tumors and ESCs (Figure 3B) (Ohta et al., 2013). We also found that the Myc module displays similar activation between Dox-withdrawn tumors and ESCs (Figure S3A). The activation of ESC-Core and ESC-Myc modules was similarly confirmed in transplanted secondary tumors (Figure S3B).

(D) Minced Dox-withdrawn tumor cells were injected in the subcutaneous tissues of immunocompromised mice. A histological section of one of the tumors phenocopied the original Dox-withdrawn tumor. Scale bars, 200 μm (upper panel) and 100 μm (lower panel).

(E) A schematic drawing of the OKS transgene at the *Col1a1* locus. A histological section of the kidney on days 21 and 28. The expansion of dysplastic cells was observed in the stomach and kidneys on day 21 (arrows). The dysplastic cell growth could be detected even after the withdrawal of Dox in OKS-induced mice (day 28). Scale bars, 200 μm.

(F) A schematic drawing of the KMS transgene. A histological section of a kidney after the treatment with Dox for 7 days (day 7) and the withdrawal of Dox for another 7 days (day 14). KMS induction leads to dysplastic growth in the kidney tubule cells (arrows for day 7). The inset shows a higher-magnification image. No dysplastic cells were detectable in the kidneys of KMS-induced mice after the withdrawal of Dox (day 14). Scale bars, 200 μm.

See also Figure S2.

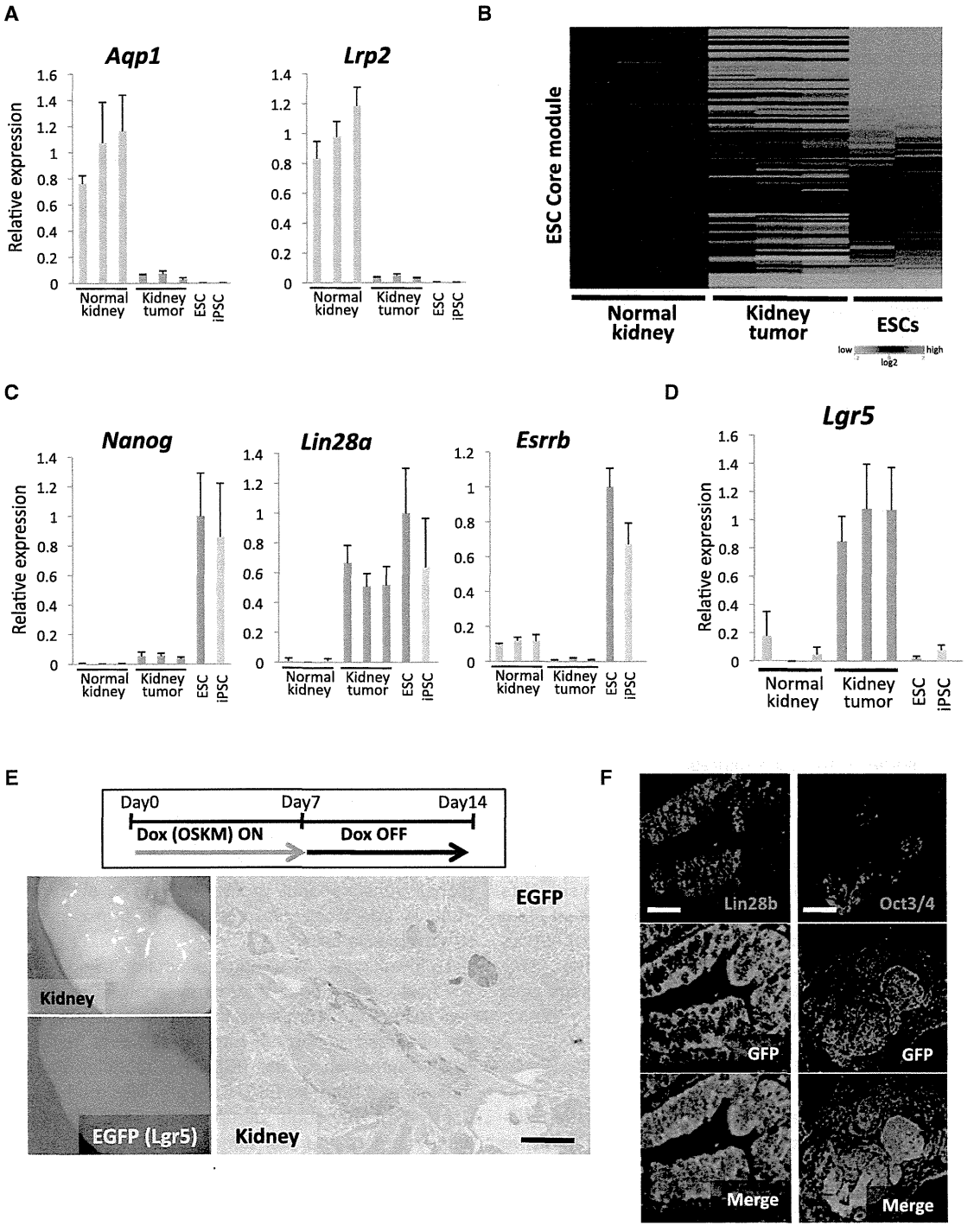

Figure 3. Loss of Cell Identity and Gain of ESC-Related Gene Expression in the Dox-Withdrawn Tumors

(A) The results of the qRT-PCR analyses of *Aqp1* and *Lrp2*. The expression levels of *Aqp1* and *Lrp2* were significantly downregulated in the Dox-withdrawn kidney tumors. Data are presented as mean ± SD. The mean level of normal kidney samples was set to 1.

(B) The microarray analyses revealed the activation of the ESC Core module in Dox-withdrawn kidney tumors.

(C) The results of the qRT-PCR analyses of pluripotency-related genes. Data are presented as mean ± SD. The transcript level in ESCs was set to 1.

(D) *Lgr5* as a candidate marker of Dox-withdrawn kidney tumor cells. *Lgr5* was specifically expressed in Dox-withdrawn kidney tumors. Data are presented as mean ± SD. The mean level of kidney tumors was set to 1.

(E) A schematic drawing of the experimental protocol using chimeric mice with both reprogrammable alleles and the *Lgr5-EGFP* allele. Macroscopic images of the Dox-withdrawn kidney tumor with the *Lgr5-EGFP* allele showing scattered EGFP signals in the kidney tumor. GFP immunostaining of kidney tumor sections revealed that the GFP signals are detectable specifically in tumor cells. Scale bar, 100 μm.

(legend continued on next page)

Some pluripotency-related genes, including *Nanog*, *Oct3/4*, and *Lin28a*, were upregulated in the Dox-withdrawn kidney tumor cells as compared to normal kidney tissue, although the expression levels of both *Nanog* and endogenous *Oct3/4* were significantly lower than that of pluripotent stem cells (Figures 3C and S3C). Conversely, other pluripotency-related genes, such as *Esrrb*, were not upregulated in these tumors (Figures 3C).

To further characterize Dox-withdrawn tumor cells, we sought to identify tumor-cell-specific markers. We found that *Lgr5* is specifically upregulated in Dox-withdrawn kidney tumor cells, but not in adult kidney tissues or pluripotent stem cells (Figure 3D). Increased expression of *Lgr5* was similarly observed in the transplanted secondary tumors (Figure S3D). Therefore, we established iPSC lines from OSKM-inducible MEFs containing *Lgr5-EGFP* reporter allele in which *Lgr5* expression can be visualized by enhanced green fluorescent protein (EGFP) (Barker et al., 2007). The established *Lgr5*-reporter iPSCs do not express EGFP in ESC culture conditions (Figure S3E). OSKM-inducible *Lgr5* reporter chimeric mice at 4 weeks of age were treated with the 7+/7− Dox regimen. Again, these mice developed Dox-withdrawn kidney tumors consisting of dysplastic cells (Figure 3E). The scattered EGFP signals were observed in kidney tumors (Figure 3E), and immunohistochemical analysis revealed that *Lgr5* is specifically expressed in part of Dox-withdrawn kidney tumor cells (Figures 3E and S3E). These findings indicate that Dox-withdrawn kidney tumors contain *Lgr5*-positive cells and that the *Lgr5* reporter allele is available to specifically identify the Dox-withdrawn kidney tumor cells that are distinct from fully reprogrammed pluripotent stem cells. Of note, some of the *Lgr5*-expressing tumor cells also expressed Oct3/4 and Lin28b in immunohistochemical analysis (Figures 3F and S3F), thus suggesting that *Lgr5*-expressing tumor cells share some characteristics with pluripotent stem cells. The fact that Dox treatment for longer than 8 days followed by Dox withdrawal often results in teratoma formation supports the notion that partial reprogramming toward pluripotent stem cells is involved in the development of Dox-withdrawn tumors (data not shown). Altogether, our findings indicate that *Lgr5*-expressing tumor cells are distinct from pluripotent stem cells but contain partially reprogrammed cells.

Failed Repression of ESC-Polycomb Targets in Dox-Withdrawn Tumors

In contrast to ESC-like activation observed for both the ESC-Core and ESC-Myc modules, the ESC Polycomb repressive complex (PRC) module was differentially expressed between Dox-withdrawn tumors and ESCs (Figure 4A). We found that a number of ESC-PRC targeted genes are not repressed in both kidney tumors and transplanted secondary tumors (Figures 4A, S4A, and S4B), indicating that the failed repression of ESC-PRC targets is associated with the development of Dox-withdrawn tumors. Consistent with the notion, more than one-forth of the upregulated genes in tumor cells as compared to ESCs (greater than 3-fold upregulation) were targets of PRC in ESCs (Mikkelsen et al., 2007) (Table S1). We also found that Dox-withdrawn kidney tumors express kidney-precursor-expressing genes such as *Six2*, *Eya1*, and *Lgr5* (Barker et al., 2012; Kobayashi et al., 2008) (Figures 4B and S4C). In particular, *Six2* and *Lgr5*, which are also PRC targets in ESCs (Mikkelsen et al., 2007), are specifically upregulated in both Dox-withdrawn kidney tumors and secondary tumors when compared to both normal kidney tissues and pluripotent stem cells (Figures 3D, 4B, S3D, and S4D). Chromatin immunoprecipitation (ChIP)-qPCR experiments confirmed decreased H3K27me3 levels at both *Six2* and *Lgr5* promoter regions in Dox-withdrawn tumors when compared with those in normal kidney tissues (Figure S4E). Failed repression of the ESC-PRC module was also detectable in unsuccessfully reprogrammed kidney cells in vitro, which were established by the transient expression of reprogramming factors in isolated kidney tubule cells in vitro (Figure S4F).

We next examined the kinetics of transcriptional changes during the development of the Dox-withdrawn tumors. Immunohistochemical analysis revealed that early dysplastic cells at day 7 coincide with transgene-expressing cells (Figure S4G). Taking advantage of florescence-linked transgene expression in our mice, we fluorescence-activated cell sorted mCherry-positive kidney cells in OSKM mice given Dox for 7 days (D7), isolating early dysplastic cells for gene expression analysis. Fluorescence-activated cell-sorted D7 LacZ-mCherry-expressing kidney cells were used as a control (Figure S4H). Decreased expression of proximal tubule cell markers was observed in the D7 OSKM cells as compared to D7 LacZ cells, suggesting that the loss of kidney cell identity occurs in early dysplastic cells (Figure S4I). In contrast, increased expression of ectopic stem/progenitor cell markers was not evident in D7 OSKM cells (Figure S4I). These findings suggest that remodeling of global transcriptional profiles toward a stem/progenitor-like state is specifically associated with transgene-independent, late dysplastic cells.

To investigate cell-of-origin effects on failed reprogramming, we next performed a microarray analysis for Dox-withdrawn liver tumors and compared the data with that of kidney tumors. As observed in kidney tumors, the liver tumors displayed failed repression of the ESC-PRC module, accompanied by activation of both the ESC-Core and Myc modules (Figure S4J; Table S1). Although derepressed PRC module genes in kidney tumors and liver tumors often overlapped (Figure S5A; Table S1), we found differentially derepressed PRC genes between kidney and liver tumors. Notably, such differentially derepressed PRC genes were associated with kidney and liver development, respectively. These findings suggest that failed PRC repression in Dox-withdrawn tumors may be associated with the activation of a developmental transcription

(F) Dox-withdrawn tumors express pluripotency-related proteins. Double immunofluorescence for Lin28b and GFP (Lgr5) revealed that the GFP-positive tumor cells also expressed Lin28b. Double immunofluorescence for Oct3/4 and GFP (Lgr5) showed that a subset of GFP-positive tumor cells expressed Oct3/4 in the nucleus. Scale bars, 20 μm.
See also Figure S3.

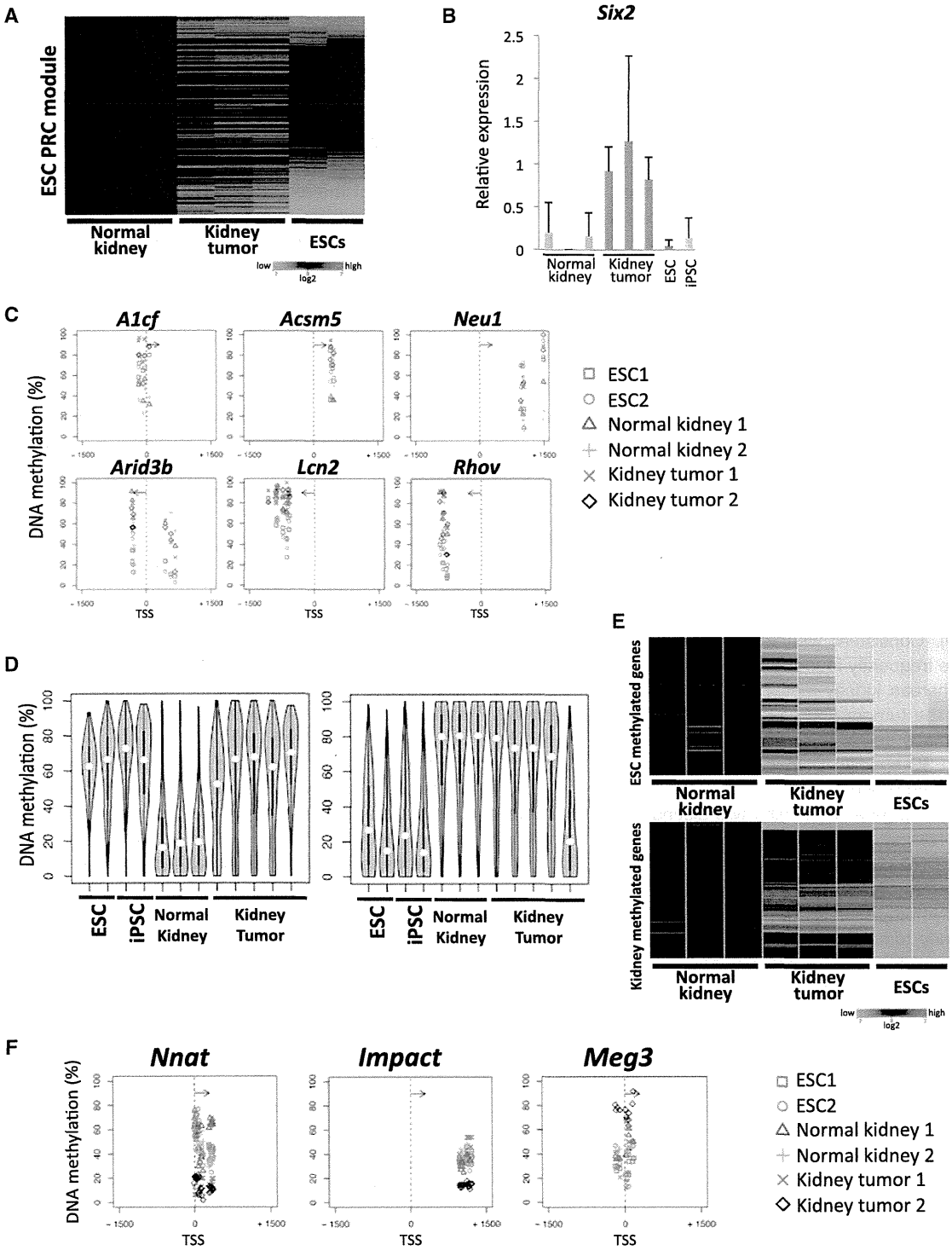

Figure 4. Altered Epigenetic Regulation in Dox-Withdrawn Tumors

(A) The microarray analyses revealed that ESC-PRC target genes were often activated in Dox-withdrawn kidney tumors compared to normal kidney tissues.

(B) *Six2* was highly expressed only in the Dox-withdrawn kidney tumors. Data are presented as mean ± SD. The mean level of kidney tumors was set to 1.

(C) Altered DNA methylation patterns in Dox-withdrawn tumors and the DNA methylation status of representative genes in the RRBS analyses.

(D) The global analyses for the DNA methylation levels. Genes that were differentially methylated between ESCs and normal kidney samples (more than 30% difference) were extracted and then analyzed for DNA methylation levels in Dox-withdrawn kidney tumors. Kidney tumors gain DNA methylation at ESC-methylated genes, whereas kidney-methylated genes often retain their methylation status in kidney tumors.

(legend continued on next page)

program, which is affected in part by the cell of origin (Figure S5A).

Altered DNA Methylation in Dox-Withdrawn Kidney Tumor Cells

Somatic cell reprogramming is accompanied by global changes in DNA methylation patterns (Mikkelsen et al., 2008). The fact that failed reprogramming can cause tumor development suggests that altered epigenetic modifications play a role in tumorigenesis. To quantitatively profile DNA methylation in Dox-withdrawn tumors, we next performed reduced representation bisulfite sequencing (RRBS) (Meissner et al., 2005). We identified a number of genes with altered DNA methylation levels in Dox-withdrawn tumors as compared to normal kidney tissues. Dox-withdrawn tumors revealed frequent gains of DNA methylation at DNA-methylated genes in ESCs, whereas loss of methylation at DNA-methylated genes in kidney tissues was not evident (Figure 4C). To validate these findings, we next performed a global analysis. We first extracted genes differentially methylated between ESCs and normal kidney samples and then examined their DNA methylation in Dox-withdrawn tumors. The global analysis confirmed that Dox-withdrawn kidney tumors gained de novo methylation at ESC-methylated genes, whereas kidney-methylated genes often retain their methylation in Dox-withdrawn kidney tumors (Figure 4D). Consistent with these findings, ESC-methylated genes were frequently found to be repressed in Dox-withdrawn tumors, whereas kidney-methylated genes tended to remain silent in these tumors (Figure 4E). These results suggest that loss of somatic cell-specific DNA methylation is preceded by a gain of ESC-specific DNA methylation patterns during the reprogramming process.

Adult cancers generally exhibit two distinct patterns of alterations in DNA methylation: site-specific DNA hypermethylation and global DNA hypomethylation (Jones and Baylin, 2002; Yamada et al., 2005). We performed specified regional analyses for the DNA methylation in normal kidney tissues and Dox-withdrawn kidney tumors. DNA hypermethylation at promoter regions in Dox-withdrawn tumors was not detectable, regardless of the presence of CpG islands (Figure S5B). Additionally, decreased DNA methylation levels at intergenic regions were not obvious in Dox-withdrawn tumors (Figure S5B).

We found that Dox-withdrawn kidney tumors aberrantly express a number of imprinted genes and that altered expression levels are similar to those in ESCs (Figure S5C). When DNA methylation status at differentially methylated regions (DMRs) of imprinted genes were examined in Dox-withdrawn tumors using a MassARRAY platform (Ehrich et al., 2005), we found frequent alterations of DNA methylation status at DMRs in Dox-withdrawn tumors (Figure S5D). The aberrant genomic methylation levels at imprinted genes in Dox-withdrawn tumors were also confirmed by RRBS analysis (Figures 4F and S5E). Intriguingly, each Dox-withdrawn tumor revealed variable aberrations in DNA methylation at different imprinted genes. The aberrant methylation includes hypermethylation at the *Meg3* (*Gtl2*) DMR, which has been correlated with impaired differentiation properties of iPSCs (Stadtfeld et al., 2010a) (Figures 4F and S5E). Moreover, SNP analysis in the hybrid KH2 background revealed that the altered expression of some imprinted genes in Dox-withdrawn tumors arise from biallelic transcription, compared to monoallelic expression in the original OSKM-inducible ESCs (Figure S5F). Collectively, these results suggest that genomic imprinting is unstable in Dox-withdrawn tumors and provide additional evidence that altered gene expression underlying tumor development is associated with altered epigenetic signatures.

Dox-Withdrawn Kidney Tumors Resemble Wilms Tumors

Histological analysis revealed that Dox-withdrawn kidney tumors in reprogrammable mice resemble Wilms tumor, the most common pediatric kidney cancer (Figure 5A). A number of studies demonstrated that increased expression of *Igf2* with DNA hypermethylation at the *H19* DMR is one of the causative and most common alterations in Wilms tumors (Ogawa et al., 1993; Steenman et al., 1994). We confirmed that Dox-withdrawn tumors express a significantly higher level of *Igf2* than noninduced tissues (Figures 5B and S6A). Moreover, consistent with altered DNA methylation at other imprinted genes, the increased methylation at the *H19* DMR was detectable in some Dox-withdrawn kidney tumors (Figure 5C).

To additionally evaluate the similarity between Dox-withdrawn kidney tumors and Wilms tumors, we next compared global gene expression patterns. We first selected genes that are upregulated more than 5-fold in Dox-withdrawn kidney tumors in comparison with noninduced kidney tissues and then assessed expression of their human orthologs in human normal kidney tissues, Wilms tumors, and human ESCs (hESCs) using previously reported microarray data sets (Tchieu et al., 2010; Yusenko et al., 2009). We found that upregulated genes in Dox-withdrawn kidney tumors are frequently upregulated in both Wilms tumors and hESCs as compared to normal kidney samples (Figure 5D), whereas this upregulation is not evident in adult kidney cancers (renal cell carcinomas [RCCs]) (Figure S6B).

We also analyzed the expression of genes in ESC-Core, ESC-Myc, and ESC-PRC modules in Wilms tumors. Notably, ESC-upregulated genes in both ESC-Core and ESC-Myc modules are similarly activated in Wilms tumors (Figures 5D and S6C), although *NANOG* and *OCT3/4* are not expressed in Wilms tumors. In contrast, a fraction of ESC-PRC targeted genes expressed in kidney progenitors, such as *SIX2* and *LGR5*, are specifically upregulated in Wilms tumors as compared with

(E) DNA-methylation-associated gene regulation in Dox-withdrawn tumors. The vast majority of ESC-methylated genes were downregulated in Dox-withdrawn tumors, whereas a significant portion of kidney-methylated genes remained repressed in these tumors. ESC-methylated genes with decreased expression levels in ESCs and kidney-methylated genes with decreased expression levels in the kidney tissues were examined.

(F) Altered DNA methylation at the DMR of imprinting genes. Note that kidney tumor 2 showed aberrant methylation patterns at *Nnat*, *Impact*, and *Meg3*. In contrast, kidney tumor 1 showed an aberration only at *Nnat*.

See also Figures S4 and S5.

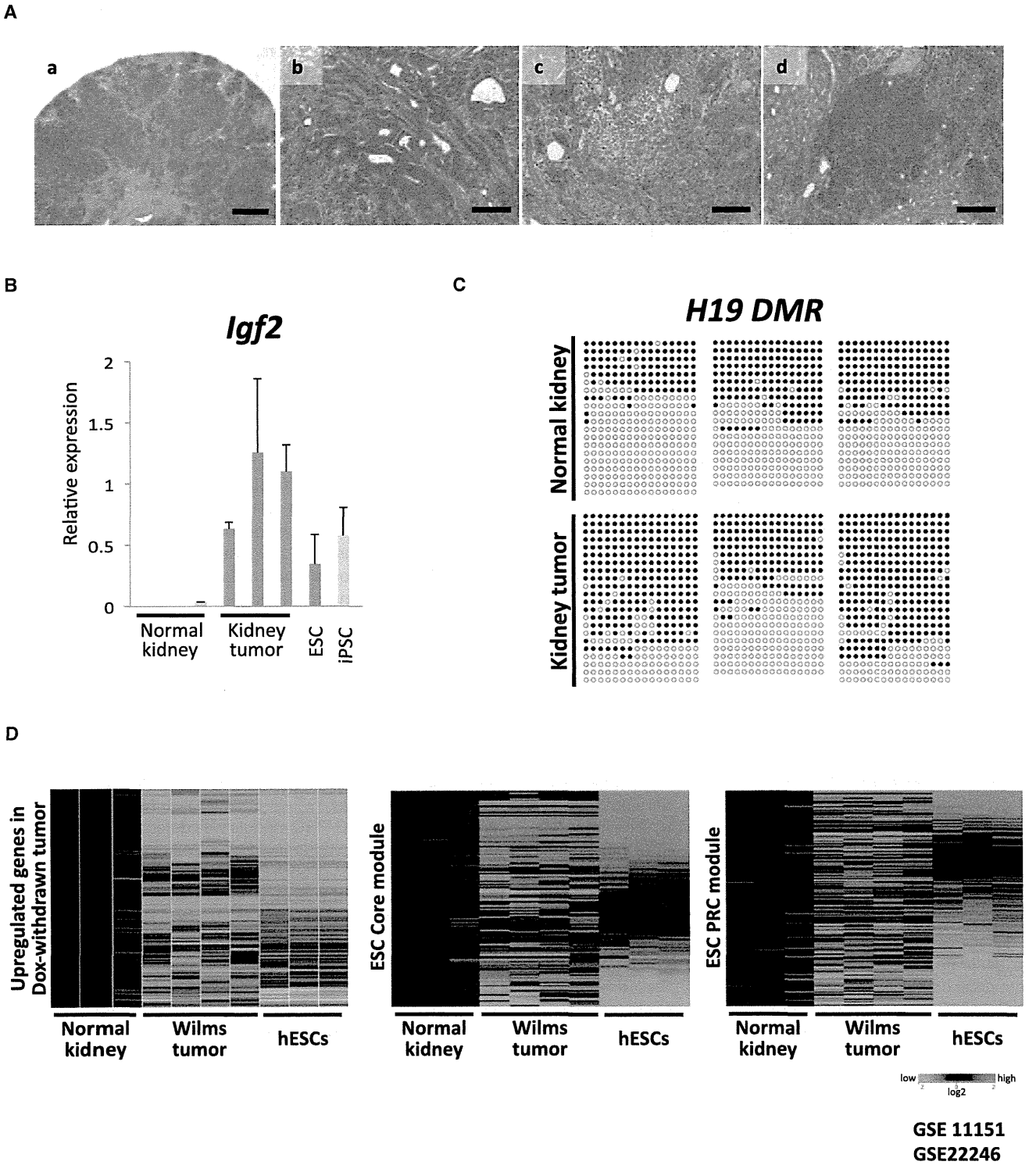

Figure 5. Dox-Withdrawn Kidney Tumors Resemble Wilms Tumors

(A) Representative histological findings of Dox-withdrawn kidney tumors (a–d). Tumors consisted of epithelial (b), stromal (c), and blastema-like (d) compartments, which are histological features of Wilms tumors. Scale bars, 500 μm (a) and 100 μm (b–d).

(B) The results of the qRT-PCR analysis for *Igf2*. *Igf2* was highly expressed in Dox-withdrawn kidney tumors. Data are presented as mean ± SD. The mean level of kidney tumors was set to 1.

(legend continued on next page)

those in normal kidney tissues, hESCs, and RCCs (Figures 5D and S6D) (Aiden et al., 2010). Collectively, kidney tumors induced by the transient expression of reprogramming factors display a number of shared characteristics with Wilms tumor. These findings also indicate that our mouse model may prove useful to uncover the pathogenesis of Wilms tumors.

iPSCs Derived from Dox-Withdrawn Kidney Tumors Contribute to Nonneoplastic Kidney Tissues in Chimeric Mice

We next tried to establish iPSCs from Dox-withdrawn kidney tumor cells. The tumor cell-specific *Lgr5-EGFP* reporter allele defined in this study was utilized to isolate tumor cells (Figures 3D, 3E, and S3E). *Lgr5*-expressing GFP-positive tumor cells were sorted and cultured in vitro with Dox to establish iPSCs from tumor cells (Figure 6A). During the culture of *Lgr5*-expressing tumor cells in vitro, *Nanog* expression at a level comparable to that in pluripotent stem cells was detected as early as 7 days after reprogramming factor induction (Figure 6B), a rate faster than the reprogramming process from normal kidney tubule cells in vitro (Figure S7A). After 2 weeks of culture with Dox exposure, more than 20 alkaline phosphatase (AP)-positive iPSC-like colonies were obtained from 100 *Lgr5*-expressing tumor cells (Figure S7B). We were able to establish Dox-independent iPSC lines from tumor cells at 3 weeks after transgene induction (Figure 6C), suggesting that the Dox-withdrawn tumor cells can be readily reprogrammed into pluripotent stem cells.

Cancers are believed to arise through the accumulation of multiple genetic abnormalities. We next investigated whether genetic abnormalities mandate the emergence of in Dox-withdrawn tumors. Exonic regions of 514 genes that include human-cancer-related genes in transplanted secondary kidney tumors were sequenced using a hybridization selection technique combined with next-generation sequencing (Table S3). Mutations in *Wt1*, *Wtx*, *Ctnnb1*, and *Trp53*, all of which have been identified in a subset of Wilms tumors, were not detected in three tumors examined. In addition, no cancer-related gene mutations were enriched in these tumors (data not shown). Array-based comparative genomic hybridization (CGH) revealed no prevalent chromosomal alteration in tumor samples (Figure S7C).

Finally, we injected the tumor-derived iPSCs into blastocysts to generate chimeric mice. Tumor-derived iPSCs contributed into adult chimeric mice (Figure 6D). Notably, the kidney-tumor-derived iPSCs differentiated into normal-looking kidney tissues (Figures 6E, 6F, and S7D). Moreover, these chimeric mice did not develop tumors even at 24 weeks of age (n = 8). To further demonstrate that tumorigenic cells can be reprogrammed into nonneoplastic cells, we also established iPSCs from the transplanted secondary tumors and confirmed their contribution to nonneoplastic kidney tissues (Figure S7E). These results substantiate that a genetic context of the Dox-withdrawn kidney tumor cells is not determinant of the cancer phenotype and support the conclusion that altered epigenetic regulations cause the abnormal growth in somatic cells, leading to the development of Dox-withdrawn tumors.

DISCUSSION

During somatic cell reprogramming, iPSCs gain the capacity for unlimited growth without particular genetic alterations. Using abbreviated reprogramming factor expression in vivo, we demonstrate that transient expression of reprogramming factors leads to tumor development. Such tumors display altered epigenetic modifications, indicating that epigenetic regulation characteristic of cellular reprogramming may also confer neoplastic growth properties to somatic cells. Intriguingly, Dox-withdrawn tumor cells are readily reprogrammed into pluripotent stem cells by additional 4F expression, indicating that the tumor cells represent a cellular state closer to iPSCs than the original somatic cells. Moreover, kidney tumor cell-derived iPSCs contribute to various somatic cell types and give rise to nonneoplastic kidney cells in mice. These data demonstrate that the abnormal growth of unsuccessfully reprogrammed cells depends predominantly on epigenetic regulations and raise the possibility that particular types of cancer may arise exclusively through altered epigenetic regulation.

Histological features of Dox-withdrawn tumors imply that unsuccessfully reprogrammed cells lack the ability to terminal differentiate along multiple lineages. It is noteworthy that Dox-withdrawn tumor cells fail to repress ESC-PRC targets yet share the activation of ESC core regulatory circuitry and Myc-related genes with pluripotent stem cells. It is conceivable that the repression of ESC-PRC targets would be exclusively associated with the acquisition of pluripotency, whereas activation of ESC core regulatory circuitry and Myc targets lead to self-renewing activity. This notion is also consistent with previous findings that PRC components are important for successful reprogramming in humans (Onder et al., 2012). Notably, the failed repression of the ESC-PRC module was detectable in previously reported partially reprogrammed cells in vitro (Polo et al., 2012), in which the activation of both ESC-Core and ESC-Myc modules had already occurred (Figure S7F). We also found that unsuccessfully reprogrammed kidney cells tend to retain DNA methylation at kidney-specific methylated genes. Considering that global epigenetic reorganization, including changes in both H3K27 methylation and DNA methylation, occurs during the later phase of iPSC generation (Polo et al., 2012), the expected repression of ESC-PRC targets and demethylation of somatic cell-specific genomic methylation might play a role in the final stages of successful somatic cell reprogramming.

Recently, Abad et al. reported that in vivo reprogramming allows the acquisition of totipotent features resulting in embryo-like cyst formation in reprogrammable mice (Abad et al., 2013). However, in the present study, we did not observe such cystic structures in Dox-treated reprogrammable mice.

(C) The bisulfite sequencing analysis revealed increased DNA methylation levels at the *H19* DMR containing two CTCF binding sites in Dox-withdrawn tumors. (D) The results of the global expression analyses in Wilms tumors. The human orthologs of upregulated genes in Dox-withdrawn tumors and ESC module genes were assessed using previously reported microarray data sets (GSE11151 and GSE22246).
See also Figure S6.

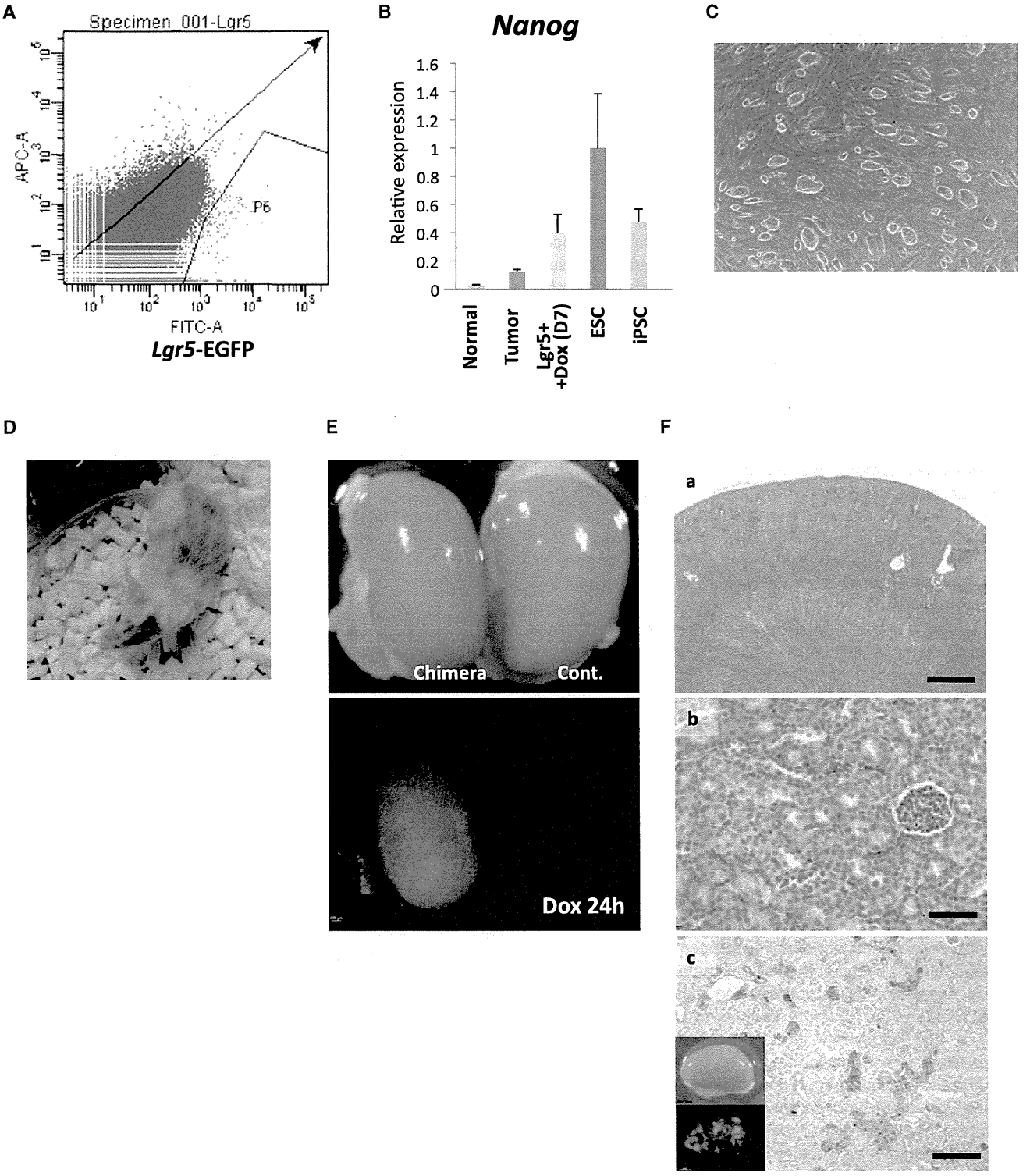

Figure 6. Generation of iPSCs from Dox-Withdrawn Tumors and Their Contribution to Normal-Looking Kidney Tissue

(A) The fluorescence-activated cell sorting analyses of Dox-withdrawn kidney tumor cells in a reprogrammable chimeric mouse with the *Lgr5*-EGFP reporter. GFP-positive *Lgr5*-expressing cells were sorted to exclusively isolate Dox-withdrawn tumor cells.

(B) Dox treatment of *Lgr5*-expressing tumor cells caused the rapid induction of *Nanog*. The *Nanog* levels were examined after seven days of treatment with Dox in vitro. Data are presented as mean ± SD. The level in ESCs was set to 1.

(C) An image of iPSCs derived from *Lgr5*-positive kidney tumor cells.

(legend continued on next page)

Furthermore, teratoma-derived in vivo iPSCs in this study failed to differentiate into placental tissues despite robust fetal contribution upon injection into eight-cell-stage embryos (data not shown), suggesting that not all in vivo iPSCs are totipotent. Because the previous study was conducted using circulating iPSCs recovered in blood, the cell of origin for in vivo reprogramming might affect the acquisition of totipotent features. It should be also noted that Abad et al. utilized germline-transmitted transgenic mice that harbor lentivirus-mediated integration of inducible reprogramming factors (Carey et al., 2009) whereas we examined chimeric mice with transgenes at a targeted locus. The different levels of transgene induction caused by such distinct transgenic systems may underlie differences in the phenotypes observed between these two studies.

Here, we show that failed reprogramming-associated cancers resemble Wilms tumors in terms of histology and molecular characteristics, including aberrant expression of imprinted genes correlated with altered DNA methylation. It is well known that Wilms tumors have characteristics distinct from adult kidney cancers in many aspects. On the basis of our findings in Dox-withdrawn tumors, we discovered that Wilms tumors harbor an activated ESC core regulatory circuitry. This is in sharp contrast to previous findings that most adult cancers do not show activation of ESC core regulatory circuitry (Kim et al., 2010). We also found that many ESC-PRC targets are not repressed in Wilms tumors, despite common repression in many cancers (Ben-Porath et al., 2008; Kim et al., 2010). Gene Ontology analysis revealed that derepressed PRC genes in Wilms tumors include genes involved in kidney development, whereas they are not enriched in derepressed PRC genes in RCCs (data not shown), suggesting that activation of the embryonic kidney transcriptional network is associated with Wilms tumor development. Taken together, strongly active ESC-core regulatory circuitry and derepression of certain ESC-PRC targets may characterize Wilms tumors and may account for the characteristics distinctive of Wilms tumors and adult kidney cancers.

Although we revealed striking similarity between Dox-withdrawn kidney tumors and Wilms tumors, it remains unclear whether reprogramming processes play a role in the development of human Wilms tumors. It has been widely accepted that nephrogenic rests, abnormally persistent clusters of embryonal cells, are the precursors of Wilms tumors. Considering the artificial expression of reprogramming factors in our experimental system, the current study does not provide direct evidence that dedifferentiation is normally involved in the human Wilms tumor development. Yet, based on our findings, it is conceivable that a reprogramming process might cause cell-fate conversion into progenitor-like states, leading to the development of nephrogenic rests required for the early stages of Wilms tumorigenesis. Further detailed analyses using human samples are required to uncover the role of reprogramming in cancer development in humans.

In summary, we demonstrated that premature termination of in vivo reprogramming causes tumor development resembling Wilms tumor. Our findings suggest that altered epigenetic regulations relating to somatic cell reprogramming drive tumorigenesis, highlighting the importance of epigenetic regulation in cancer development.

EXPERIMENTAL PROCEDURES

Generation of OSMK-Inducible ESCs

A 7 kb fragment containing Oct3/4-P2A-Sox2-T2A-Klf4-E2A-c-Myc-ires-mCherry cDNA was generated (Carey et al., 2009) and ligated into the pBS31 vector (Beard et al., 2006). The resulting construct was electroporated into KH2 ESCs to obtain OSKM-inducible ESCs (Beard et al., 2006). OKS-, KMS-, O-, LacZ-inducible ESCs were also generated using the KH2 ESCs system.

Mice

Chimeric mice were generated using reprogramming factor-inducible ESCs by diploid blastocyst injection. *Lgr5-EGFP-ires-CreERT2* mice were obtained from The Jackson Laboratory and were crossed with OSKM-inducible mice to obtain embryos. The compound transgenic MEFs were treated with Dox to establish the OSKM-inducible iPSCs with the *Lgr5-EGFP* reporter allele. All animal experiments were approved by the CiRA Animal Experiment Committee, and the care of the animals was in accordance with institutional guidelines.

Doxycycline Treatment

Mice at 4 or 14 weeks of age were administered 2 mg/ml Dox in their drinking water supplemented with 10 mg/ml sucrose. For cell culture, Dox was used at a concentration of 2 μg/ml.

Secondary Tumor Development

Primary kidney tumors were minced and treated with collagenase (1 U/ml) followed by 0.25% trypsin digestion. The dissociated tumor cells were inoculated subcutaneously into BALB/cSlc-*nu/nu* mice or C.B-17/Icr-*scid*Jcl mice to form transplanted secondary tumors.

RNA Preparation, qRT-PCR and Microarray Analysis

Total RNA was isolated using the RNeasy Plus Mini kit (QIAGEN). The quantitative real-time PCR analysis was performed using the GoTaq qPCR Master Mix (Promega). The specific primer pairs used for amplification are shown in Table S2. The transcript levels were normalized to the *β-actin* level. The microarray analysis was performed using the Mouse Gene 1.0 ST Array (Affymetrix) in accordance with the manufacturer's instructions. All of the data analyses were performed using the GeneSpring GX software program (version 12; Agilent Technology).

DNA Methylation Analyses

The RRBS analysis was performed as described previously (Boyle et al., 2012). The samples were sequenced on an Illumina HiSeq 2000 machine. Three-kilobase regions flanking transcription start site (from −1,500 to +1,500) were analyzed to examine DNA methylation levels. The DNA methylation levels for each gene were determined based on the median of DNA methylation values at CpG sites within the region. The DNA methylation values at CpG sites

(D) Kidney tumor-derived iPSCs can contribute to adult chimeric mice.
(E) No tumor formation was observed in the kidneys of chimeric mice generated with kidney tumor-derived iPSCs. Note that Dox treatment for 24 hr confirmed the contribution of kidney-tumor-derived iPSCs to the normal-looking kidney.
(F) The histological analyses of the kidneys of chimeric mice demonstrated no detectable histological abnormalities (a and b). Kidney-tumor-derived iPSCs labeled with Venus could contribute to normal-looking kidney (c). Scale bars, 500 μm (a) and 100 μm (b, c).
See also Figure S7.

containing higher than 10× coverage in all comparative samples were used for the analysis.

Histological Analysis and Immunostaining

Normal and tumor tissue samples were fixed in 10% buffered formalin for 24 hr and embedded in paraffin. Sections (4 μm) were stained with hematoxylin and eosin (H&E), and serial sections were used for the immunohistochemical analyses. The primary antibodies used were anti-Oct3/4 (1:100 dilution; BD Biosciences), anti-Ki-67 (1:100 dilution; Dako), anti-insulin (1:500 dilution; Dako), anti-BrdU (1:500 dilution; Abcam), anti-2A (1:250 dilution; Millipore), anti-Lin28b (1:100 dilution; Cell Signaling Technology), and anti-GFP (1:500 dilution; Invitrogen).

ACCESSION NUMBERS

The Gene Expression Omnibus accession number for the microarray and RRBS data reported in this paper is GSE52304.

SUPPLEMENTAL INFORMATION

Supplemental Information includes Extended Experimental Procedures, seven figures, and three tables and can be found with this article online at http://dx.doi.org/10.1016/j.cell.2014.01.005.

ACKNOWLEDGMENTS

We are grateful to T. Taya for CGH analysis and S. Sakurai and T. Sato for RRBS analysis. We also thank S. Masui, H. Sakurai, and members in Yamada laboratory for helpful discussions and T. Ukai, K. Osugi, and N. Nishimoto for assistance. The authors were supported in part by a Grant-in-Aid from the Ministry of Education, Culture, Sports, Science, and Technology of Japan (MEXT); the Ministry of Health, Labor, and Welfare of Japan; the JST; the Funding Program for World-Leading Innovative R&D on Science and Technology (FIRST Program) of the Japanese Society for the Promotion of Science (JSPS); the Takeda Science Foundation; and the Naito Foundation. S.Y. is a member without salary of the scientific advisory boards of iPierian, iPS Academia Japan, Megakaryon Corporation, and HEALIOS K. K. Japan. The iCeMS is supported by World Premier International Research Center Initiative, MEXT, Japan.

Received: May 29, 2013
Revised: November 6, 2013
Accepted: January 3, 2014
Published: February 13, 2014

REFERENCES

Abad, M., Mosteiro, L., Pantoja, C., Cañamero, M., Rayon, T., Ors, I., Graña, O., Megías, D., Domínguez, O., Martínez, D., et al. (2013). Reprogramming in vivo produces teratomas and iPS cells with totipotency features. Nature *502*, 340–345.

Aiden, A.P., Rivera, M.N., Rheinbay, E., Ku, M., Coffman, E.J., Truong, T.T., Vargas, S.O., Lander, E.S., Haber, D.A., and Bernstein, B.E. (2010). Wilms tumor chromatin profiles highlight stem cell properties and a renal developmental network. Cell Stem Cell *6*, 591–602.

Barker, N., van Es, J.H., Kuipers, J., Kujala, P., van den Born, M., Cozijnsen, M., Haegebarth, A., Korving, J., Begthel, H., Peters, P.J., and Clevers, H. (2007). Identification of stem cells in small intestine and colon by marker gene Lgr5. Nature *449*, 1003–1007.

Barker, N., Rookmaaker, M.B., Kujala, P., Ng, A., Leushacke, M., Snippert, H., van de Wetering, M., Tan, S., Van Es, J.H., Huch, M., et al. (2012). Lgr5(+ve) stem/progenitor cells contribute to nephron formation during kidney development. Cell Rep. *2*, 540–552.

Beard, C., Hochedlinger, K., Plath, K., Wutz, A., and Jaenisch, R. (2006). Efficient method to generate single-copy transgenic mice by site-specific integration in embryonic stem cells. Genesis *44*, 23–28.

Ben-Porath, I., Thomson, M.W., Carey, V.J., Ge, R., Bell, G.W., Regev, A., and Weinberg, R.A. (2008). An embryonic stem cell-like gene expression signature in poorly differentiated aggressive human tumors. Nat. Genet. *40*, 499–507.

Boyle, P., Clement, K., Gu, H., Smith, Z.D., Ziller, M., Fostel, J.L., Holmes, L., Meldrim, J., Kelley, F., Gnirke, A., and Meissner, A. (2012). Gel-free multiplexed reduced representation bisulfite sequencing for large-scale DNA methylation profiling. Genome Biol. *13*, R92.

Brambrink, T., Foreman, R., Welstead, G.G., Lengner, C.J., Wernig, M., Suh, H., and Jaenisch, R. (2008). Sequential expression of pluripotency markers during direct reprogramming of mouse somatic cells. Cell Stem Cell *2*, 151–159.

Carey, B.W., Markoulaki, S., Hanna, J., Saha, K., Gao, Q., Mitalipova, M., and Jaenisch, R. (2009). Reprogramming of murine and human somatic cells using a single polycistronic vector. Proc. Natl. Acad. Sci. USA *106*, 157–162.

Carey, B.W., Markoulaki, S., Beard, C., Hanna, J., and Jaenisch, R. (2010). Single-gene transgenic mouse strains for reprogramming adult somatic cells. Nat. Methods *7*, 56–59.

Ehrich, M., Nelson, M.R., Stanssens, P., Zabeau, M., Liloglou, T., Xinarianos, G., Cantor, C.R., Field, J.K., and van den Boom, D. (2005). Quantitative high-throughput analysis of DNA methylation patterns by base-specific cleavage and mass spectrometry. Proc. Natl. Acad. Sci. USA *102*, 15785–15790.

Folmes, C.D., Nelson, T.J., Martinez-Fernandez, A., Arrell, D.K., Lindor, J.Z., Dzeja, P.P., Ikeda, Y., Perez-Terzic, C., and Terzic, A. (2011). Somatic oxidative bioenergetics transitions into pluripotency-dependent glycolysis to facilitate nuclear reprogramming. Cell Metab. *14*, 264–271.

Fussner, E., Djuric, U., Strauss, M., Hotta, A., Perez-Iratxeta, C., Lanner, F., Dilworth, F.J., Ellis, J., and Bazett-Jones, D.P. (2011). Constitutive heterochromatin reorganization during somatic cell reprogramming. EMBO J. *30*, 1778–1789.

Hochedlinger, K., Yamada, Y., Beard, C., and Jaenisch, R. (2005). Ectopic expression of Oct-4 blocks progenitor-cell differentiation and causes dysplasia in epithelial tissues. Cell *121*, 465–477.

Hong, H., Takahashi, K., Ichisaka, T., Aoi, T., Kanagawa, O., Nakagawa, M., Okita, K., and Yamanaka, S. (2009). Suppression of induced pluripotent stem cell generation by the p53-p21 pathway. Nature *460*, 1132–1135.

Jones, P.A., and Baylin, S.B. (2002). The fundamental role of epigenetic events in cancer. Nat. Rev. Genet. *3*, 415–428.

Kim, J., Woo, A.J., Chu, J., Snow, J.W., Fujiwara, Y., Kim, C.G., Cantor, A.B., and Orkin, S.H. (2010). A Myc network accounts for similarities between embryonic stem and cancer cell transcription programs. Cell *143*, 313–324.

Kobayashi, A., Valerius, M.T., Mugford, J.W., Carroll, T.J., Self, M., Oliver, G., and McMahon, A.P. (2008). Six2 defines and regulates a multipotent self-renewing nephron progenitor population throughout mammalian kidney development. Cell Stem Cell *3*, 169–181.

Maherali, N., Sridharan, R., Xie, W., Utikal, J., Eminli, S., Arnold, K., Stadtfeld, M., Yachechko, R., Tchieu, J., Jaenisch, R., et al. (2007). Directly reprogrammed fibroblasts show global epigenetic remodeling and widespread tissue contribution. Cell Stem Cell *1*, 55–70.

Meissner, A., Gnirke, A., Bell, G.W., Ramsahoye, B., Lander, E.S., and Jaenisch, R. (2005). Reduced representation bisulfite sequencing for comparative high-resolution DNA methylation analysis. Nucleic Acids Res. *33*, 5868–5877.

Mikkelsen, T.S., Ku, M., Jaffe, D.B., Issac, B., Lieberman, E., Giannoukos, G., Alvarez, P., Brockman, W., Kim, T.K., Koche, R.P., et al. (2007). Genome-wide maps of chromatin state in pluripotent and lineage-committed cells. Nature *448*, 553–560.

Mikkelsen, T.S., Hanna, J., Zhang, X., Ku, M., Wernig, M., Schorderet, P., Bernstein, B.E., Jaenisch, R., Lander, E.S., and Meissner, A. (2008). Dissecting direct reprogramming through integrative genomic analysis. Nature *454*, 49–55.

Ogawa, O., Eccles, M.R., Szeto, J., McNoe, L.A., Yun, K., Maw, M.A., Smith, P.J., and Reeve, A.E. (1993). Relaxation of insulin-like growth factor II gene imprinting implicated in Wilms' tumour. Nature *362*, 749–751.

Ohta, S., Nishida, E., Yamanaka, S., and Yamamoto, T. (2013). Global splicing pattern reversion during somatic cell reprogramming. Cell Rep. *5*, 357–366.

Okita, K., Ichisaka, T., and Yamanaka, S. (2007). Generation of germline-competent induced pluripotent stem cells. Nature *448*, 313–317.

Onder, T.T., Kara, N., Cherry, A., Sinha, A.U., Zhu, N., Bernt, K.M., Cahan, P., Marcarci, B.O., Unternaehrer, J., Gupta, P.B., et al. (2012). Chromatin-modifying enzymes as modulators of reprogramming. Nature *483*, 598–602.

Polo, J.M., Anderssen, E., Walsh, R.M., Schwarz, B.A., Nefzger, C.M., Lim, S.M., Borkent, M., Apostolou, E., Alaei, S., Cloutier, J., et al. (2012). A molecular roadmap of reprogramming somatic cells into iPS cells. Cell *151*, 1617–1632.

Rais, Y., Zviran, A., Geula, S., Gafni, O., Chomsky, E., Viukov, S., Mansour, A.A., Caspi, I., Krupalnik, V., Zerbib, M., et al. (2013). Deterministic direct reprogramming of somatic cells to pluripotency. Nature *502*, 65–70.

Samavarchi-Tehrani, P., Golipour, A., David, L., Sung, H.K., Beyer, T.A., Datti, A., Woltjen, K., Nagy, A., and Wrana, J.L. (2010). Functional genomics reveals a BMP-driven mesenchymal-to-epithelial transition in the initiation of somatic cell reprogramming. Cell Stem Cell *7*, 64–77.

Sridharan, R., Tchieu, J., Mason, M.J., Yachechko, R., Kuoy, E., Horvath, S., Zhou, Q., and Plath, K. (2009). Role of the murine reprogramming factors in the induction of pluripotency. Cell *136*, 364–377.

Stadtfeld, M., Apostolou, E., Akutsu, H., Fukuda, A., Follett, P., Natesan, S., Kono, T., Shioda, T., and Hochedlinger, K. (2010a). Aberrant silencing of imprinted genes on chromosome 12qF1 in mouse induced pluripotent stem cells. Nature *465*, 175–181.

Stadtfeld, M., Maherali, N., Borkent, M., and Hochedlinger, K. (2010b). A reprogrammable mouse strain from gene-targeted embryonic stem cells. Nat. Methods *7*, 53–55.

Steenman, M.J., Rainier, S., Dobry, C.J., Grundy, P., Horon, I.L., and Feinberg, A.P. (1994). Loss of imprinting of IGF2 is linked to reduced expression and abnormal methylation of H19 in Wilms' tumour. Nat. Genet. *7*, 433–439.

Takahashi, K., and Yamanaka, S. (2006). Induction of pluripotent stem cells from mouse embryonic and adult fibroblast cultures by defined factors. Cell *126*, 663–676.

Takahashi, K., Tanabe, K., Ohnuki, M., Narita, M., Ichisaka, T., Tomoda, K., and Yamanaka, S. (2007). Induction of pluripotent stem cells from adult human fibroblasts by defined factors. Cell *131*, 861–872.

Tchieu, J., Kuoy, E., Chin, M.H., Trinh, H., Patterson, M., Sherman, S.P., Aimiuwu, O., Lindgren, A., Hakimian, S., Zack, J.A., et al. (2010). Female human iPSCs retain an inactive X chromosome. Cell Stem Cell *7*, 329–342.

Wernig, M., Meissner, A., Foreman, R., Brambrink, T., Ku, M., Hochedlinger, K., Bernstein, B.E., and Jaenisch, R. (2007). In vitro reprogramming of fibroblasts into a pluripotent ES-cell-like state. Nature *448*, 318–324.

Woltjen, K., Michael, I.P., Mohseni, P., Desai, R., Mileikovsky, M., Hämäläinen, R., Cowling, R., Wang, W., Liu, P., Gertsenstein, M., et al. (2009). piggyBac transposition reprograms fibroblasts to induced pluripotent stem cells. Nature *458*, 766–770.

Yamada, Y., Jackson-Grusby, L., Linhart, H., Meissner, A., Eden, A., Lin, H., and Jaenisch, R. (2005). Opposing effects of DNA hypomethylation on intestinal and liver carcinogenesis. Proc. Natl. Acad. Sci. USA *102*, 13580–13585.

Yusenko, M.V., Kuiper, R.P., Boethe, T., Ljungberg, B., van Kessel, A.G., and Kovacs, G. (2009). High-resolution DNA copy number and gene expression analyses distinguish chromophobe renal cell carcinomas and renal oncocytomas. BMC Cancer *9*, 152.

特集　周産期胎盤の診断病理

間葉性異形成胎盤placental mesenchymal dysplasia (PMD)の診断と原因遺伝子

大場　隆[*1]　片渕秀隆[*1]
副島英伸[*2]

はじめに

間葉性異形成胎盤placental mesenchymal dysplasia (PMD)は，胞状奇胎と類似した嚢胞状変化を呈するが，組織学的にはtrophoblastの異常増殖を認めない稀な胎盤形態異常である．部分胞状奇胎や胎児共存奇胎との鑑別が重要であるとともに，早産，胎児発育不全，胎児死亡を高率に合併する高リスク妊娠でもある．一方，PMD発生原因については，ゲノムインプリンティングの異常やVEGF遺伝子の関与が示唆されている．本稿ではPMDの臨床と原因遺伝子について最新の知見を基に解説する．

Ⅰ．PMDの臨床

1．PMDの疫学

1990年代に入って，超音波断層法にて胎盤の嚢胞状変化を呈し，組織学的に胞状奇胎とは異なる胎盤の形態異常が報告され始めた．diffuse stem villous hyperplasia[1]，placentomegaly with massive hydrops of placental stem villi[2]など，様々な呼称が提唱されてきたが，現在では間葉性異形成胎盤placental mesenchymal dysplasia (PMD)の語が定着している．PMDは稀な病態であり，2007年までの英文文献による症例報告は約70例[3]，また2010年までの本邦における症例報告は30余例だが，実際の頻度は4,000～5,000妊娠に1例と推定され[4]，この病態の認識が広まるにつれて本邦での報告例も増えている．妊娠中の超音波断層法スクリーニングがなく，PMDの疾患概念が普及していなかった時代には，原因不明の巨大胎盤としてPMDの診断に至らなかった症例が相当数あるものと推定される．現在我々は本邦におけるPMD症例の解析を進めており，以下はこれまでに集積した32症例の検討に基づいている．

PMDの児は女児が多いこと，さらにPMDの児の25%がBeckwith-Wiedemann症候群(BWS)を呈することから[5]，PMDの発症にはインプリンティング機構が関与していることが示唆されてきた．この詳細は本稿の後半で触れる．近年，生殖補助医療assisted reproductive technology(ART)がインプリンティング異常症のリスクを増大させている可能性が指摘されているが[6,7]，PMDに関してはその影響は乏しいようである．PMDの発症に関わる因子は今後の大規模な前向き調査で検討される必要がある．

2．PMDの診断

PMDの診断基準は確立していない．娩出された胎盤の肉眼所見から疑われるか，あるいは妊娠初期の超音波断層法で部分胞状奇胎や胎児共存奇胎との鑑別に挙げられることが診断の契機となる(**表1**)．

超音波断層法では胎児が認められ，胎盤は肥厚して実質内に大小不整な嚢胞や管腔様構造を呈する(**図1a,b**)．MRIでは，全体的に肥厚した単葉の胎盤が観察され，内部には大小の嚢胞状構造が散在している．超音波断層法所見はPMDを疑う契機として重要であるが，我々が集積したPMD症例のうち，妊娠初期の超音波断層法で胞状奇胎様の構造を指摘されたものは62.5%(20/32)にとどまっており，超音波断層法で所見がないことはPMDを除外する根拠とはならない．さらに超音波断層法における嚢胞や管腔様構造は妊娠経過とともに目立たなくなる可能性が指摘されている．

我々の検討では，母体血中ヒト絨毛性ゴナドトロピンが異常高値を示した症例は約20%で，いずれも一過性の上昇であり妊娠中期以降には減少した．一方，母体血中α-フェトプロテインは測定が行われた症例

[*1]熊本大学大学院生命科学研究部 産科婦人科学分野
[*2]佐賀大学医学部分子生命科学講座 分子遺伝学・エピジェネティクス分野

0287-3745/14/¥100/頁/JCOPY

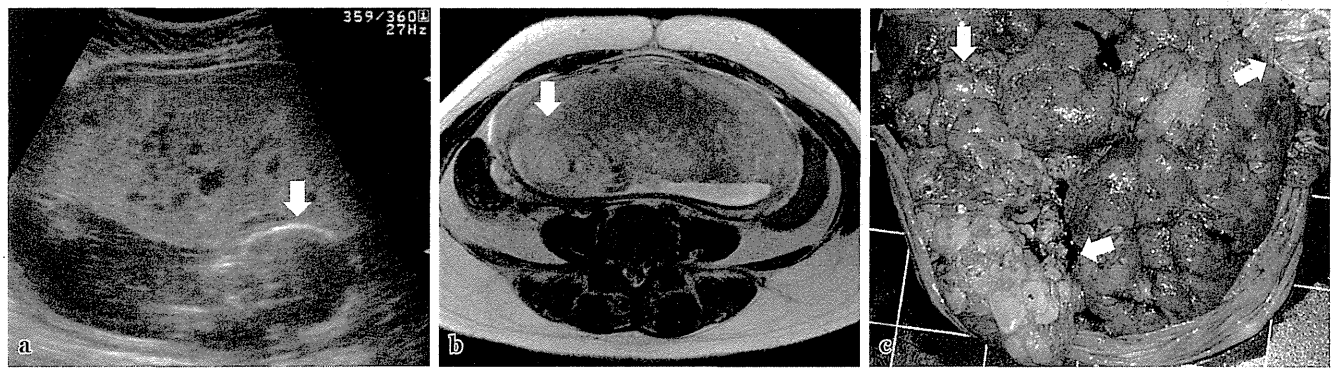

図1　間葉性異形成胎盤(PMD)の画像診断と肉眼所見　a：経腹超音波断層法(妊娠17週5日)，b：MRI T2強調画像(妊娠18週0日)．胎児(矢印)とともに肥厚した胎盤が認められる．胎盤は均質で胎児面は平滑，実質内に大小不整な嚢胞や管腔様構造を認める．c：肉眼所見．妊娠31週2日，出生体重1,116 g，胎盤重量450 g，胎盤胎児重量比0.40．胎盤の胎児面には多嚢胞状の部位(矢印)と変化の乏しい部位が混在している．(北海道大学産科・周産母子センター　山田崇弘博士より提供)

表1　PMDと胞状奇胎の鑑別点(文献3より改変)

	胎児共存奇胎	部分胞状奇胎	間葉性異形成胎盤(PMD)
核型	diploid(正常胎盤＋全胞状奇胎)	triploid	diploid
胎児	正常	三倍体による子宮内胎児死亡	BWS(20%)，胎児発育不全(20%)，子宮内胎児死亡(30%)
母体血中hCG	高値	高値	正常/軽度高値(40%)
母体血中AFP	高値	高値	高値
USG/MRI所見	正常絨毛領域とmultivesicle領域が明瞭に区別される	一様にmultivesicle	巨大な胎盤，multivesicle様の大小不整な管腔
病理組織学所見	trophoblastの異常増殖	trophoblastの異常増殖	幹絨毛血管の動脈瘤様拡張
$p57^{KIP2}$発現	cytotrophoblastに陰性	cytotrophoblastに陽性	絨毛内の間質・血管に陰性
母体続発症	絨毛存続症/絨毛癌	絨毛存続症/絨毛癌	なし

全てが高値を示し，特に第2三半期で高値(各症例の極大値は中央値625 ng/mL(141～7,310 ng/mL))であった．

PMDは一見して巨大な胎盤であることが特徴とされてきたが，PMDでは早産に至ることが多いため，重量が1,000 gを超える，いわゆる巨大胎盤となる症例は約半数にとどまっていた．一方，胎盤/胎児重量比は，中央値0.48(0.23～1.92)と高い値を示しており，相対的な巨大胎盤であることがこの病態を疑わせる指標として重要と考えられる．胎盤の母体面には，一見して胞状奇胎を連想させる多数の嚢胞を認め，その周辺には怒張，蛇行した血管が認められる．このような変化は胎盤の一部または複数箇所に限局して認められることが多い(**図1c**)．

病理組織学評価には，中山の提唱した基準が参考となる[8](**表2**)．水腫様の絨毛には血管があるがtrophoblastの異常な増殖はない．蛇行した絨毛血管内に間葉系細胞の増生があり多発性の血栓がみられる．PMDでは$p57^{KIP2}$蛋白は細胞性栄養膜細胞にのみ発現し，絨毛内の間質や血管は$p57^{KIP2}$陰性である[9]．このような病理組織学的所見は同じ胎盤であっても採取部位によって差異が大きく，注意すべき点と思われる．

3. PMDと妊娠異常

図2に我々が集積した症例の在胎週数と出生体重の分布を示す．分娩に至った31症例は，早産83.8%(26/31)，極低出生体重児出生38.7%(12/31)，子宮内胎児死亡intrauterine fetal death(IUFD)16.1%(5/31)，帝王切開率71.0%(22/31)といずれも高率で，PMDの妊娠は高リスク妊娠となることが改めて明らかとなった．BWSの児はBWSを伴わない児に比べると出生体重が大きい傾向はあるが必ずしも巨大児ではなかった．